University of Alberta

Nanostructured Environmental Barrier Coatings for Corrosion
Resistance in Recovery Boilers

by

Shishir Rao

A thesis submitted to the Faculty of Graduate Studies and Research
in partial fulfillment of the requirements for the degree of

Master of Science

Department of Mechanical Engineering

Abstract

Corrosion of components in a recovery boiler is a major problem faced by the pulp and paper industry. The superheater tubes get severely corroded due to the presence of hot sulphidic gases in the boiler as well as the hot molten salts which get deposited on the surface of the tubes. As a result, the boiler has to be shut down for expensive maintenance and repairs. This thesis examines the possibility of using air plasma sprayed (APS) yttria-stabilized zirconia (YSZ) environmental barrier coatings (EBC) to protect against molten salt corrosion of superheater tubes. Conventional YSZ and nanostructured YSZ samples were prepared and exposed to different environments to check their resistance to corrosion. The performances of both types of coatings were evaluated and a comparative study was made. It was found that the nanostructured YSZ samples protected the stainless steel substrate better than the its conventional counterpart. This superior performance was attributed to the presence of semi-molten nano agglomerates present in the coating microstructure which act as collection bags for the penetrating molten salts.

Acknowledgements

Table of Contents

List of Figures

List of Tables

1. Introduction

1.1 Background

Recovery boilers in the pulp and paper industry are large fuel-to-energy boilers designed to combust organic waste from the pulping process [1]. Although they are very similar to other boilers that burn coal, municipal waste and wood waste, what differentiates a recovery boiler from the others is their function as a chemical reactor [2]. The primary function of a recovery boiler is to recover the spent inorganic cooking chemicals and convert them into forms suitable for reuse in the pulping process [1]. Black-liquor is a by-product of the *Kraft* process, which is used to make paper, and it is the fuel used for combustion in a recovery boiler. The steam and heat energy produced as a result of combustion of black liquor in a recovery boiler is used as process steam in the *Kraft* process, as well as to generate auxiliary electricity that is used by the plant. Combustion of black liquor fuel results in the formation of hot, sulphidic gases, which corrode the boiler surfaces and tubes. Corrosion of components in a recovery boiler is a major challenge faced by the pulp and paper industry. It limits the overall energy efficiency of the boiler, largely due to restrictions placed on maximum steam temperatures to prevent molten salt corrosion of the superheater tubes. Also, the hot molten pool of inorganic salts at the bottom of the boiler reacts with water to create a very energetic and often catastrophic explosion [3]. This smelt − water

explosion is purely a physical phenomenon. Even a few liters of water when mixed with the molten smelt causes the water to evaporate and turn into steam within a fraction of a second. This sudden evaporation of water causes a sudden increase in volume and a pressure wave of 10,000 – 100,000 Pa. This force is unidirectional and is sufficient enough to bend the boiler walls. As a result, the boiler has to be shut down for expensive maintenance.

1.2 Thermal Spraying

Thermal spraying is a process where micron sized ceramic, metal or alloy particles are melted and accelerated to build a thick protective coating on industrial machine components. The principle of thermal spraying is shown in Fig. 1. As shown in the figure, the process consists of a spray gun to which the coating powder is supplied. Flame spray, air plasma spray (APS) and high velocity oxy-fuel (HVOF) are a few of the different thermal spray processes used in the industry for coating machine components. The thermal spray guns differ for different processes. In this study, the air plasma spraying process was used to prepare the thermal sprayed samples. A schematic diagram of the air plasma spraying process is shown in Fig. 2. In this process, a strong electric arc is generated between a positively charged electrode (anode) and a negatively charged electrode (cathode). The approximate arc temperature is around 16,000^{o}C. This temperature is enough to melt ceramics with high melting points and hence atmospheric plasma spray process is best suited for depositing ceramic coatings.
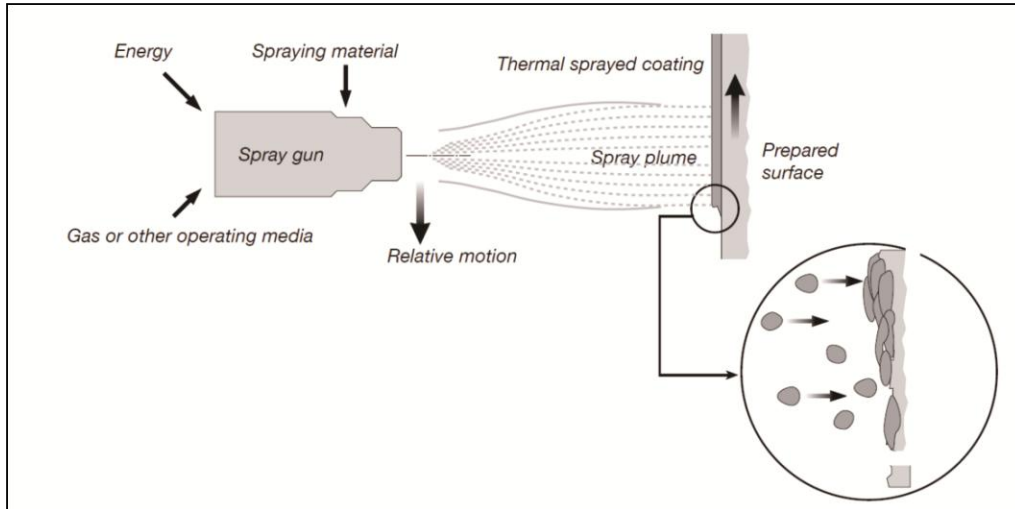
Figure 1: Principle of thermal spraying [4]
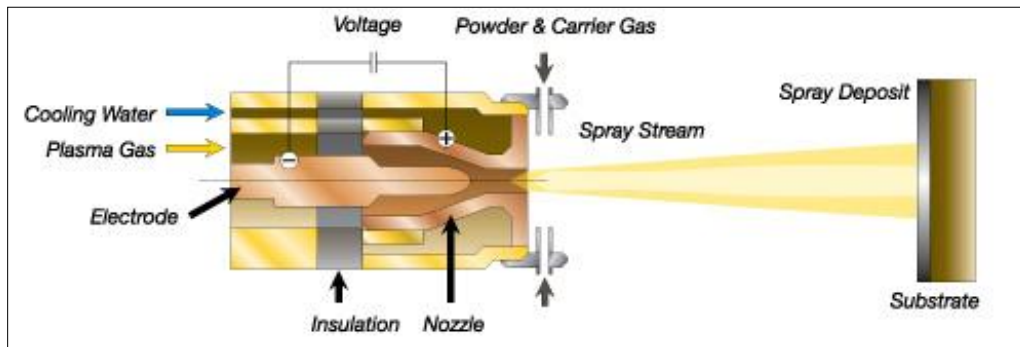
Figure 2: Atmospheric plasma spraying [4].

Plasma gases are used to generate the plasma jet. A primary gas (typically argon or nitrogen) and a secondary gas (helium and/or hydrogen) together constitute the plasma gas. The strong electric arc generated ionizes the process gases into a plasma state. Powder feedstock material is injected into the plasma jet by a carrier gas, melting the powder and accelerating it towards the substrate. The molten powder impacts and spreads on the substrate surface and forms a layer of coating. The spray gun (or torch) is usually mounted on a robot, which is

programmed to move relative to the substrate during the spraying process. The thickness of the coating to be deposited is determined by the number of passes or repetitions the robot makes across the substrate.

The power supplied to the spray gun can be controlled, giving the opportunity to control the amount of energy transferred to the feedstock powder. The spray gun continuously exchanges heat with cooling water so that the gun does not overheat due to the plasma.

The density of thermal sprayed coatings depends on the size of the powder particles. The amount of porosity increases with the increase in the particle size [5]. Hence, small particle plasma spraying would result in a coating with fewer cracks and pores. This would be beneficial in preventing penetration of corrosive gases though the coating.

The substrates are grit blasted before they are ready to be sprayed. Grit blasting is a process in which the substrates are blasted with abrasive pellet particles. These particles remove surface oxides and contaminants stuck to the surface of the substrates. Grit blasting also roughens the surface, thereby promoting increased adhesion of the deposited coating. For thermal spraying, aluminum oxide grit is typically used. Grit blasting is done in a closed chamber where the grit pellets are projected at a high speed through a nozzle towards the substrate.

1.3 Application of Ceramic Coatings to Gas Turbines

Gas turbines typically operate at temperatures above 1370°C. At such temperatures, the turbine superalloy blades are affected by structural failures like

creep, oxidation, thermal fatigue and even melting. One way to protect these blades is by using a ceramic thermal barrier coating (TBC). Yttria-stabilized zirconia(YSZ) coatings have been proved to extend the durability of gas turbine engine combustors due to the superior thermal insulation provided by the YSZ ceramic [6]. The thermal insulation also allows higher operating temperatures and reduced cooling requirements in gas turbines, thereby increasing the efficiency of the engine. These coatings have also shown to provide erosion and corrosion resistance in gas turbines [7]. Thermal barrier coatings generally consist of two coats - a bond coat and a top coat. The bond coat is applied directly on top of the substrate. Nickel-Chromium-Cobalt-Aluminium-Yttria (NiCrCoAlY) or Nickel-Chromium-Aluminium-Yttria (NiCrAlY) are widely used as bond coat material for YSZ coatings. The top coat is the actual ceramic (YSZ) and is deposited on top of the bond coat. The metallic bond coat performs two functions (a) to provide oxidation resistance and (b) to adhere the ceramic physically to the underlying superalloy structure [6]. The YSZ top coat is an oxygen transparent layer i.e. YSZ is an excellent oxygen ion conductor. The oxygen is transferred through ionic diffusion through the crystalline structure of ZrO_2 and gas penetration through porosities and micro cracks. During gas turbine operations which occur at a high temperature, a thermally grown oxide (TGO) layer is formed between the bond coat and the YSZ interface. This layer acts as a resistant layer against further oxidation [8]. Also, a large thermal expansion mismatch exists between the superalloy substrate and the ceramic YSZ top coat. Applying the top coat directly on top of the superalloy may cause the coating to peel off due to this mismatch.

Thus, the presence of a bond coat also helps the ceramic top coat to adhere physically to the substrate. A typical bond coat is 75 to 150 μm thick while an APS top coat is 300 μm thick [9].

Until recently, conventional YSZ has been a standard feedstock powder for the top coat of a TBC. This powder is spray dried and densified forming the so called hollow spherical powder (HOSP). The HOSP method, a proprietary method similar to plasma spheroidization, is a rapid solidification process and the time the material has to homogenize in the flame is short. This leads to chemical inhomogeneities even within one feedstock grain. Nanostructured YSZ is a recently engineered material, developed as an alternative to conventional fused/crushed YSZ. Nanostructured materials are those which exhibit grain sizes that are less than 100 nm in at least one dimension [10]. The nanostructured coating microstructure has a bimodal feature, consisting of a structure formed by resolidification of the agglomerates that are fully molten in the spray jet and the semi molten agglomerates known as nano-zone areas [11]. The thermal diffusivity of nanostructured YSZ coatings have been measured to be lower than the conventional YSZ coatings [11]. It has also been shown that the thermal shock resistance of nano YSZ coating is 2-4 times higher than that of the conventional material [12]. High temperature exposure leads to an increase in the size of the particles located in the nanozone areas, thereby healing the nanoporosity contained within the nanozones [12]. These positive features make nano YSZ the preferred choice for TBC material in gas turbines.

It has also been reported that nanostructured coatings tend to be tougher than their conventional counterparts [12]. One of the hypotheses employed to explain this enhanced toughness is the crack arresting behaviour of the nanozones present in the microstructure of the coating [12]. A coating where the vertical cracks do not propagate through to the substrate and are arrested by the nanozones would prove to be very beneficial in the case where they are applied on superheater tubes. Corrosive, sulphidic gases present in a recovery boiler may penetrate these coatings through the cracks and reach the substrate, thereby corroding them.

Nanostructured powders are extremely fine particles and hence cannot be sprayed directly using the conventional thermal spray equipment. The fine particles would clog the powder carrying hoses, which carry powder from the powder feeder to the spray gun. In addition, (a) to inject individual nanoparticles into a spray jet would require high levels of carrier gas flow - the gas that transports powder from the powder hopper to spray gun, which would tend to destabilize the thermal spray jet, and (b) individual nanoparticles would tend to exhibit low inertial levels, which would make the deposition process inefficient [12]. Thus, in order to spray nano particles, they are first agglomerated via spray drying to form micro - particles which can then be sprayed using the conventional method. Figure 3 shows an example of spray dried and agglomerated nanostructured YSZ [12]. The microscopic YSZ particle shown in Fig. 3a was formed by the agglomeration (spray drying) of individual nano-sized YSZ
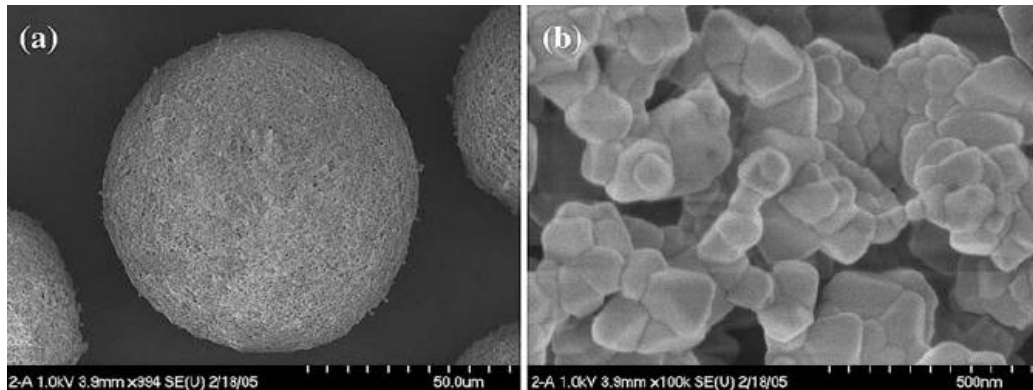
Figure 3: (a) YSZ feedstock particle formed by the agglomeration of individual nano-particles (b) Particle of (a) observed at higher magnification showing individual nano sized YSZ particles. [12]

particles shown in Fig. 3b. While air plasma spraying nanostructured YSZ powder, it is important to control carefully the spray parameters so as not to completely melt the powder and preserve part of the nanostructure of the agglomerates in the coating microstructure.

During plasma spraying of YSZ environmental barrier coatings, a non transformable tetragonal phase (called *t'* to distinguish it from the equilibrium, transformable *t* phase) is formed due to the high quenching rate of the process [13]. The phase diagram of YSZ is shown in Fig. 4 [14]. From the diagram, we can see that at room temperature, ZrO_2 containing 8% by mass Y_2O_3 (8.7 mol% $YO_{1.5}$) should have a tetragonal phase. But rapid solidification occurs during plasma spraying and this results in the formation of metastable phases – phase composition equivalent to that for some higher temperature. [15]. This metastable *t'* phase should have the same yttria content as the feedstock powder while the equilibrium tetragonal phase (*t*) should have lower yttria content (from phase diagram). Previous work has shown that as-sprayed YSZ coatings mainly consists

of high-yttria metastable tetragonal phase (*t'*) (89.6 %) and traces of the low yttria tetragonal phase (*t*), cubic phase (*c*) and monoclinic phases (*m*) [16].

The *t'* phase does not undergo the martensitic transformation to the monoclinic phase. The transformation between the tetragonal (*t*) and monoclinic (*m*) is accompanied by a volume change (approx 3~5 vol%) [17]. This change in volume is detrimental to the integrity of the coating as it causes cracking and may lead to failure of the coating due to the thermal expansion co-efficient mismatch with the substrate. Hence, the *t'* phase is the most desirable phase in YSZ coatings.
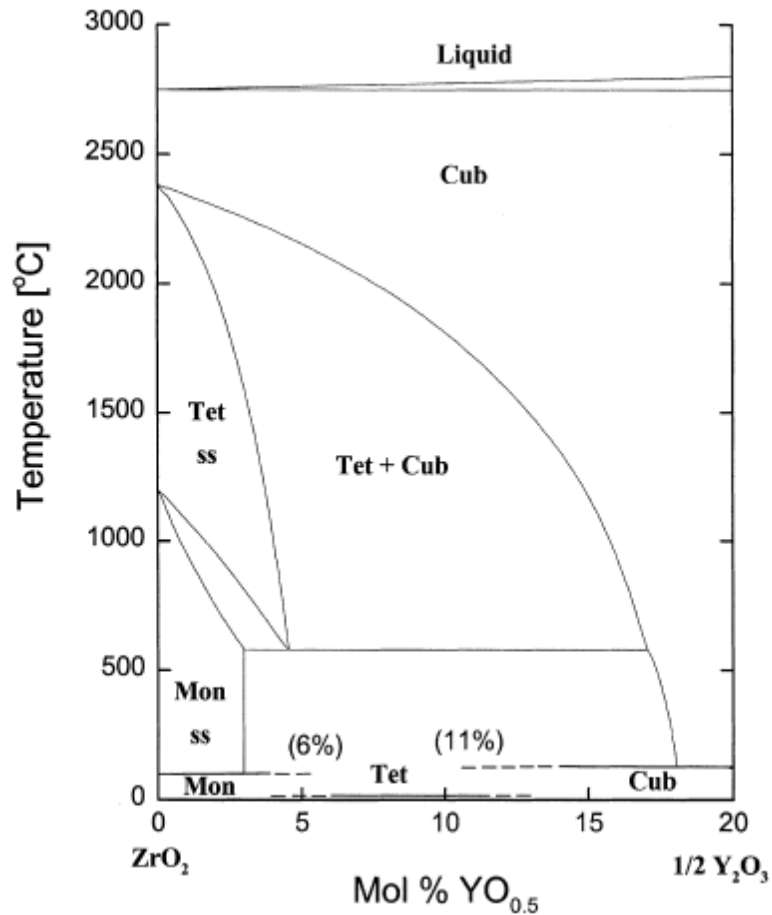
Figure 4: Phase diagram of YSZ [14]

Various studies have been conducted on phase changes in YSZ after annealing them at temperatures above 1000°C [13,15,16,18]. All these studies show that the metastable *t'* phase is unstable at such high temperatures and decomposes into the low yttria tetragonal *t* phase and cubic phase. A study by Muraleedharan *et al.* shows that after heat treating as-sprayed coatings at 1250°C for 25 hrs, the metastable *t'* phase decomposes, giving rise to tetragonal and cubic phases [13]. In a recovery boiler, the coatings would be exposed only to 600°C and hence phase transformation is not expected at this temperature. Thus, the metastable *t'* phase from the as-sprayed condition should be retained. In this study, this has been confirmed by conducting X Ray diffraction analysis of all the samples after corrosion tests.

1.4 Focus of current study

The present study aims to explore the possibility of using the air plasma sprayed nanostructured environmental barrier coatings (EBC) as a corrosion resistant coating for superheater tubes in recovery boilers.

Based on the success of nanostructured YSZ thermal barrier coatings to resist corrosion and erosion in gas turbines, the potential for this coating to act as a barrier to corrosion in the superheater section of a recovery boiler was investigated. An EBC that provides good corrosion resistance and crack resistance would help in reducing the maintanence times of recovery boilers which operate for long durations (4 to 6 months). All thermal sprayed samples were prepared at the Thermal Spray Shop in the Department of Mechanical Engineering at the University of Alberta. High temperature exposures (600°C) of these samples

under various environments were conducted at FP Innovations - PAPRICAN in Vancouver.

Chapter 2 explores the effects of the YSZ coating on the heat transfer process in the superheater section of a recovery boiler. YSZ is a ceramic that has a very low thermal conductivity (0.8 W/m-K for a plasma sprayed nanostructured YSZ top coat [19]). This could affect the transfer of heat to the steam flowing inside the superheater tubes. A heat transfer model was prepared and the results have been discussed.

A preliminary study was conducted in Chapter 3 to understand the effects of NaCl salt on conventional and nanostructured YSZ coupons exposed at a temperature of 600°C for 76 hours.

Chapter 4 investigates the performance of the EBC when exposed to molten salts and boiler flue gases to a temperature of 600°C for a period of 168 hours.

1.5 **References**

[1]   D. Singbeil, "Corrosion in Recovery Boilers," *ASM Handbook*, vol. 13C, 2006, pp. 762-802.

[2]   T.N. Adams, W.J. Frederick, T.M. Grace, M. Hupa, K. Lisa, A.K. Jones, and H. Tran, *Kraft Recovery Boilers*, 1997.

[3]   H. Dykstra, "Recovery Boiler Corrosion Problems," *ASM Handbook*, vol. 13C, 2006, pp. 762-802.

[4]   "Thermal Spraying," *Sulzer Metco*, 2008. [Online] Available: www.sulzermetco.com.

[5]   S. Deshpande, A. Kulkarni, S. Sampath, and H. Herman, "Application of image analysis for characterization of porosity in thermal spray coatings and correlation with small angle neutron scattering," *Surface and Coatings Technology*, vol. 187, Oct. 2004, pp. 6-16.

[6]   S.M. Meier and D.K. Gupta, "The Evolution of Thermal Barrier Coatings in Gas Turbine Engine Applications," *Journal of Engineering for Gas Turbines and Power*, vol. 116, 1994, p. 250.

[7]   A.S. Osyka, A.I. Rybnikov, S.A. Leontiev, N.V. Nikitin, and I.S. Malashenko, "Experience with metal/ceramic coating in stationary gas turbines," *Surface and Coatings Technology*, vol. 76-77, Nov. 1995, pp. 86-94.

[8]   M. Saremi, A. Afrasiabi, and A. Kobayashi, "Bond Coat Oxidation and Hot Corrosion Behavior of Plasma Sprayed YSZ Coating on Ni Superalloy," *Transactions of JWRI*, vol. 36, 2007, p. 41–45.

[9]   N.P. Padture, M. Gell, and E.H. Jordan, "Thermal barrier coatings for gas-turbine engine applications.," *Science (New York, N.Y.)*, vol. 296, Apr. 2002, pp. 280-4.

[10]   C.C. Koch, *Nanostructured Materials—Processing, Properties, and Applications*, Norwich, NY: Noyes Publications, William Andrew Publishing, 2002.

[11]   R.S. Lima and B.R. Marple, "Nanostructured YSZ thermal barrier coatings engineered to counteract sintering effects," *Materials Science and Engineering: A*, vol. 485, Jun. 2008, pp. 182-193.

[12]   R. Lima and B. Marple, "Thermal Spray Coatings Engineered from Nanostructured Ceramic Agglomerated Powders for Structural, Thermal

Barrier and Biomedical Applications: A Review," *Journal of Thermal Spray Technology*, vol. 16, 2007, pp. 40-63.

[13]   K. Muraleedharan, J. Subrahmanyam, and S.B. Bhaduri, "Identification of t'Phase in ZrO_2-7.5 wt% Y_2O_3 Thermal-Barrier Coatings," *Journal of the American Ceramic Society*, vol. 71, 1988, pp. 226-227.

[14]   H.G. Scott, "Phase relationships in the zirconia-yttria system," *Journal of Materials Science*, vol. 10, Sep. 1975, pp. 1527-1535.

[15]   J. Ilavsky, "Phase composition and its changes during annealing of plasma-sprayed YSZ," *Surface and Coatings Technology*, vol. 127, May. 2000, pp. 120-129.

[16]   G. Di Girolamo, C. Blasi, L. Pagnotta, and M. Schioppa, "Phase evolution and thermophysical properties of plasma sprayed thick zirconia coatings after annealing," *Ceramics International*, vol. 36, Dec. 2010, pp. 2273-2280.

[17]   J. Moon, H. Choi, and C. Lee, "Cooling rate effects on the phase transformation of ZrO_2 base thermal barrier coatings coated by APS," *Journal of Ceramic Processing Research*, vol. 1, 2000, p. 69–73.

[18]   I.R. Gibson and J.T.S. Irvine, "Qualitative X-ray Diffraction Analysis of Metastable Tetragonal (t′) Zirconia," *Journal of the American Ceramic Society*, vol. 84, Mar. 2001, pp. 615-618.

[19]   J. Wu, H.-bo Guo, L. Zhou, L. Wang, and S.-kai Gong, "Microstructure and Thermal Properties of Plasma Sprayed Thermal Barrier Coatings from Nanostructured YSZ," *Journal of Thermal Spray Technology*, vol. 19, Aug. 2010, pp. 1186-1194.

2 Impact of YSZ Thickness on Average Fluid Temperature in Superheater Tubes

2.1 Introduction

Superheater tubes in a recovery boiler are exposed to extremely corrosive environments, which ultimately lead to their failure [1,2]. Thermal-sprayed yttria-stabilized zirconia (YSZ) coatings have been shown to provide corrosion protection when used as thermal barrier coatings on high-temperature jet engine blades [3]. Applying these coatings on superheater tubes may provide resistance against corrosion. But, YSZ coatings have very low thermal conductivity, and this might affect the heat transfer to steam flowing inside the superheater tubes. The following chapter analyzes the impact of thermal-sprayed yttria-stabilized zirconia (YSZ) coating on the heat transfer in the superheater section of a recovery boiler.

2.2 **Nomenclature**

D   Diameter (m)

f   Darcy friction factor

h   heat transfer coefficient

$(Wm^{-2}K^{-1})$

k   thermal conductivity

$(Wm^{-1}K^{-1})$

L   Length (m)

Nu   Nusselt number, $Nu = hD/k$

Pr   Prandtl Number

q   Heat flux (Wm^{-2})

Re   Reynolds number,

     $Re = \rho VD/\mu$

r   radius (m)

T   temperature (^{o}C)

V   Velocity (ms^{-1})

ε roughness (m)

μ dynamic viscosity (Pa.s)

ρ density $(kg\ m^{-3})$

Subscripts

C   ceramic

i   inner

M   bond coat + steel

m,flue   mean flue gas condition

m,steam   mean steam condition

o   outer

s   steel

surface,out   outside surface of tube

critical   critical value

2.3 **Mathematical Model**

A one-dimensional heat transfer model, in cylindrical co-ordinates, was used to calculate the total amount of heat transferred from the flue gases to the steam flowing through the superheater tubes in a recovery boiler. This value was first calculated without a protective coating(bare steel tube). Then, a heat transfer model was developed for a case where the superheater tube was coated with yttria-stabilized zirconia to calculate the change in steam temperature after the application of the coating. To keep the model as accurate as possible, it was important to find fire-side and water-side temperatures in the same recovery boiler instead of gathering data from different sources. Hence, data was used from the study by Kawaji, *et al.* [4]

Case I: Bare Steel Tube
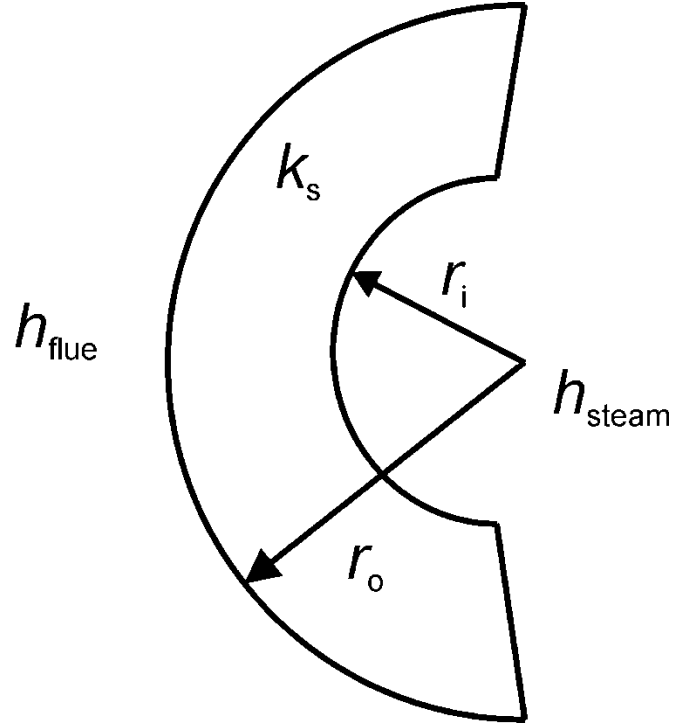
Figure 1: Section of a superheater tube**.**

The governing equation for one dimensional heat transfer in cylindrical co-ordinates is

$$\frac{\partial}{\partial r}\left(r\frac{\partial T_s}{\partial r}\right)=0 \qquad \text{for } r_i \leq r \leq r_o \tag{1}$$

The following assumptions were made in the analysis:

a. Steady state

   The average run time for recovery boilers between outages for water washes is 4 to 6 months. Hence, the assumption that heat transfer occurs at a steady state is justified.

b. Negligible axial conduction in pipe for $r_o - r_i \ll L.$

c. Uniform surface heat flux from flue gases.

In actual practice, rows of superheater tubes are placed one behind the other, forming a tube bank. Therefore, the flue gases do not come into contact with the tubes uniformly across the whole circumference. But, the main purpose of this exercise is to compare the heat transfer process with and without the coating. Hence, the assumption of uniform surface heat flux will not affect our analysis.

d. h_{flue} might be too low to assume that as $h_{\text{flue}} \to \infty, T_{\text{surface,out}} = T_{\text{flue}}$

This assumption will be justified later after the calculation of h_{flue}.

e. Pipe material is stainless steel type 304.

The boundary conditions are:

1. $k_s \dfrac{\partial T_s(r_i)}{\partial r} = \bar{h}_{\text{steam}}\left[T_s(r_i) - T_{\text{m,steam}}\right]$ \hfill (2)

2. $-k_s \dfrac{\partial T_s(r_o)}{\partial r} = \bar{h}_{\text{flue}}\left[T_s(r_o) - T_{\text{m,flue}}\right],$ \hfill (3)

where $\bar{h}$ is the average heat transfer coefficient that will be determined from appropriate heat convection correlation equations.

Heat transfer at the inner and outer surfaces of the tube take place by forced convection and radiation. Radiation heat transfer is ignored. This is because all the superheater tubes will be covered with deposits and hence the amount of heat absorbed due to radiation will be the same for a bare steel tube as well as a tube coated with YSZ. As the purpose of this exercise is to compare the amount of heat

18

transferred through a bare steel tube and a tube coated with YSZ, this assumption is justified. The two boundary conditions represent the conservation of energy at these two inner and outer boundaries. The governing equation is solved by simple integration and the solution is:

$$T_s(r) = A \ln r + B \tag{4}$$

where A and B are the constants of integration.

We find the two constants A and B by applying the two boundary conditions:

$$A = \frac{T_{m,flue} - T_{m,steam}}{\ln\left(\dfrac{r_o}{r_i}\right) + \dfrac{k_s}{r_i \bar{h}_{steam}} + \dfrac{k_s}{r_o \bar{h}_{flue}}} \tag{5}$$

$$B = \frac{k_s A}{r_i \bar{h}_{steam}} - A \ln r_i + T_{m,steam} \tag{6}$$

Now, we will need to calculate the heat transfer coefficients of the steam side as well as that of the flue gas side in order to find the constants, A and B.

A. Determination of $\bar{h}_{steam}$

Consider superheated steam flowing through the tube at a temperature of 440°C [4] and at a pressure of 625 psig [5]. The properties of steam at these conditions are shown in the table below [6]:

Table 1: Properties of steam**.**

k [W/mK]	Pr	ρ[kg/m^3]	μ[μ Pa.s]
0.006302	0.96787	13.7311	26.1081

The velocity of steam varies from 10.2 m/s to 25.4 m/s [7]. We choose 25.4 m/s since the steam velocity will be highest at the hottest section of the superheater.

The tube dimensions [4] and the average roughness, ε for Schedule 80 commercial stainless steel [8] are shown in the table below:

Table 2: Dimensions and roughness of tube.

r_o[mm]	r_i[mm]	ε[mm]
22.25	17.65	0.046

The Reynolds number was calculated to be 4.71×10^5. This means that the steam flow inside the tube is turbulent. Thus, we can apply the Gnielenski equation [9] to calculate the heat transfer coefficient of steam.

$$Nu_D = \frac{\bar{h}_{steam} D_i}{k_{steam}} = \frac{\left(\dfrac{f}{8}\right)(Re_D - 1000)Pr}{1 + 12.7\left(\dfrac{f}{8}\right)^{0.5}\left(Pr^{\frac{2}{3}} - 1\right)} \tag{7}$$

Where f is the Darcy friction factor. Equation (7) applies for the following conditions

- Developing or fully developed turbulent flow.
- Smooth tubes

$$2300 < Re_D < 5 \times 10^6$$

$$0.5 < Pr < 2000$$

$$0 < \frac{D}{L} < 1$$

The Darcy friction factor is found using Haaland's equation [10]

$$\frac{1}{\sqrt{f}} = -1.8\log\left[\frac{6.9}{Re_D} + \left(\frac{\frac{\varepsilon}{D_i}}{3.7}\right)^{1.11}\right] \tag{8}$$

After finding f from Eq. (8), it was used in Eq. (7) to find the Nusselt number and subsequently, the heat transfer co-efficient of steam was calculated. These calculated values are shown in the table below:

Table 3: Friction factor, Nusselt number and heat transfer co-efficient.

f	Nu_D	$\bar{h}_{steam}$ [W/m²-K]
4.048×10^{-3}	232	414

B. Determination of $\bar{h}_{flue}$

The superheater section in a recovery boiler consists of rows of tubes placed one behind the other to form a tube bank. Complex methods will be required to calculate $\bar{h}_{flue}$ for such a case. These methods would include determining the flue gas flow field in the superheater region using computational fluid dynamics and then using this information to find the heat transfer co-efficient. Hence, as an estimate, we model flow over one superheater pipe as flow over a cylinder. From the Churchill and Bernstein correlation equation [11], we have

$$Nu_D = \frac{\bar{h}_{flue}D_o}{k_{flue}} = 0.3 + \frac{0.62 Re_D^{\frac{1}{2}} Pr^{\frac{1}{3}}}{\left[1 + \left(\frac{0.4}{Pr}\right)^{\frac{2}{3}}\right]^{\frac{1}{4}}}\left[1 + \left(\frac{Re_D}{282000}\right)^{\frac{5}{8}}\right]^{\frac{4}{5}} \tag{9}$$

Since the mass air to fuel ratio in a boiler burner is high to promote complete combustion of fuel, we can assume that the flue gas has properties of air. The flue gas velocity is 2 m/s [12] and the temperature is 700°C [4] at atmospheric pressure. Properties of air [13] at these conditions are shown in the table below:

Table 4: Properties of flue gas.

k [W/mK]	Pr	ρ[kg/m^3]	μ[μ Pa.s]
0.06630	0.7003	0.3627	40.827

Using these properties, the Reynolds number is calculated. This value is then used in Eq. (9) to find the Nusselt number and the heat transfer co-efficient of the flue gas. These values are shown in the table below:

Table 5: Reynolds number, Nusselt number and heat transfer co-efficient.

Re_D	Nu_D	$\bar{h}_{flue}$ [W/m^2-K]
791	14.15	21.09

The heat transfer co-efficient of the flue gas is calculated to be 21.091 W/m^2-K. This justifies our previously made assumption that $\bar{h}_{flue}$ might be too low to assume $T_{surface,out} = T_{flue}$

Since the heat transfer co-efficients are now known, we can now calculate the two constants A and B from Eqs. (5) and (6). The thermal conductivity of stainless steel type 304 (at 500°C) is 21.5 W/m-K [14]. The values of A and B are 5.3072^{o}C and 477.042^{o}C. Heat flux at the outer surface of the pipe is given by:

Case II: Steel Tube coated with NiCrAlY bond coat and YSZ top coat
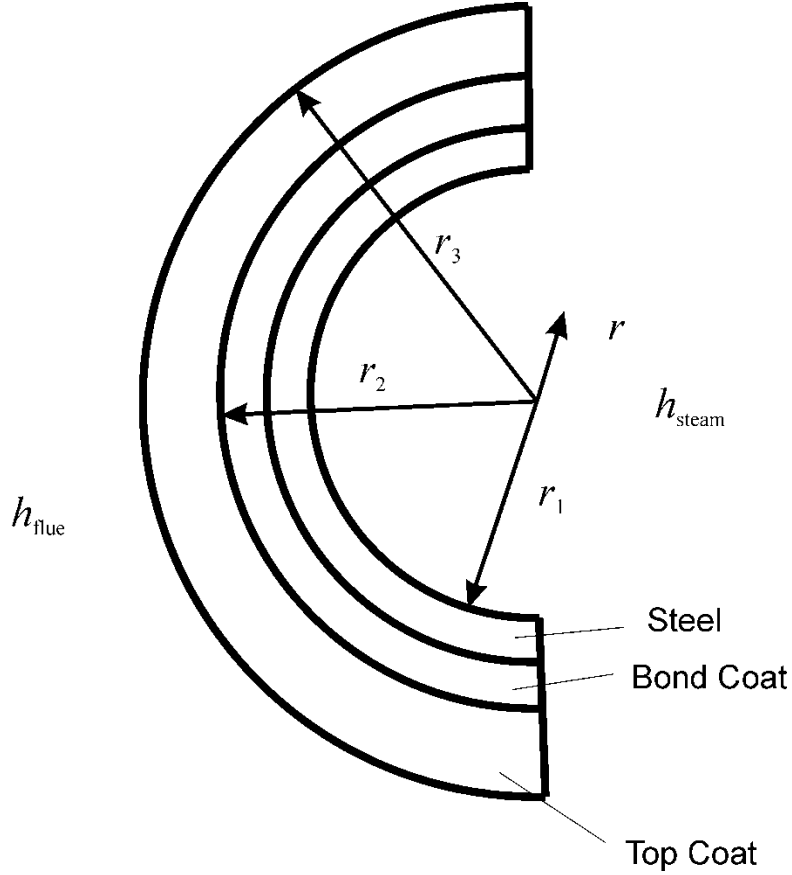
Figure 2: Section of the superheater tube with the thermal barrier coating.

$$q = -k_s \frac{\partial T_s (r_o)}{\partial r} = -k_s \frac{A}{r_o} = -5.128 \text{ kW} / \text{m}^2 \tag{10}$$

The value of heat flux is negative because the heat flows in the negative radial direction i.e. towards the centre of the superheater tube.

The following assumptions are made in the analysis

a. Steady state

b. Negligible axial conduction in pipe for $r_o - r_i \ll L$.

c. Uniform surface heat flux from flue gases.

   The above three assumptions have the same justifications as in case I.

d. Bond coat contains Ni, Cr, Al, Co and Y. The steel substrate also contains all these elements except Y. Hence, they both should have similar thermal properties. Moreover, at 600°C, the bond coat (NiCrAlY) has a thermal conductivity of around 18 W/m-K [15], which is close to the thermal conductivity of stainless steel Type 304 (21.5 W/m-K). Hence, the assumption $k_{steel} \approx k_{bond\ coat}$ is justified.

e. The gas turbine industry uses a top coat of thickness of 250 to 300 microns and a bond coat thickness of 100 to 150 microns [16]. Hence, we used the same standards in this analysis. We assumed a bond coat thickness of 100 microns and top coat thickness of 300 microns.

Therefore,

Metal inner radius = r_1 = 17.65 mm

Bond coat outer radius = r_2 = Metal outer radius + bond coat thickness = 22.25 mm + 100μm = 22.35mm

Ceramic outer radius = r_3= Bond coat outer radius + top coat thickness = 22.35 mm + 300 μm= 22.65 mm

We now have two governing equations, one for the steel + metallic bond coat and the other for the ceramic top coat.

$$\frac{\partial}{\partial r}\left(r\frac{\partial T_M}{\partial r}\right) = 0 \qquad for\ r_1 \leq r \leq r_2 \tag{11}$$

$$\frac{\partial}{\partial r}\left(r\frac{\partial T_C}{\partial r}\right) = 0 \qquad for\ r_2 \leq r \leq r_3 \tag{12}$$

The boundary conditions are:

1. $\quad k_M \dfrac{\partial T_M(r_1)}{\partial r} = \bar{h}_{steam}\left[T_M(r_1) - T_{m,steam}\right]$ (13)

2. $\quad k_C \dfrac{\partial T_c(r_3)}{\partial r} = \bar{h}_{flue}\left[T_{m,flue} - T_C(r_3)\right] = -q$ (14)

3. $\quad T_M(r_2) = T_C(r_2)$ (15)

4. $\quad k_M \dfrac{\partial T_M(r_2)}{\partial r} = k_C \dfrac{\partial T_C(r_2)}{\partial r}$ (16)

Eqs. (11) and (12) are solved by simple integration and the solutions are:

$$T_M(r) = A\ln r + B \tag{17}$$

$$T_C(r) = C\ln r + D \tag{18}$$

Thermal conductivity of plasma sprayed nanostructured YSZ top coat at 700°C = 0.8 W/m-K [17].

It is already known that the value of the term q appearing in Eq. (14) is -5.128 kW/m^2, since it was calculated in Case I. Using this information and the boundary conditions of Eqs. (14),(15) and (16), we were able to calculate the values of the four constants of integration A(5.4022°C), B(475.449°C), C(145.1865°C) and D(1006.7593°C). Having calculated all the constants, we used this information in boundary condition 1 to calculate the temperature of steam and this value was found to be 438°C.

Hence, the steam temperature has decreased to 437.745^{o}C from 440°C after the application of the EBC. This is a decrease of only 0.5 %. We can therefore conclude that the coating has had negligible impact on heat transfer in the superheater section.

2.4 Comment

The thermal conductivity of a plasma sprayed nanostructured YSZ top coat is lower than its conventional counterpart owing to its higher porosity. While the nanostructured YSZ has a thermal conductivity of 0.8 W/m-K at 700°C, the conventional one has a thermal conductivity of 1.6 W/m-K at the same temperature [17]. A similar analysis was performed with a conventional YSZ top coat and it was found that the steam temperature dropped from 440°C to 439°C.

2.5 Conclusion

The heat transfer model in the above chapter shows that there is negligible impact of the nanostructured YSZ coating on the heat transfer process in a recovery boiler. Hence, the application of such a coating to mitigate corrosion of superheater tubes might be a good solution to the problem of tube failures.

2.6 **References**

[1]   B.J. Skrifvars, R. Backman, M. Hupa, K. Salmenoja, and E.Vakkilainen, "Corrosion of superheater steel materials under alkali salt deposits Part 1: The effect of salt deposit composition and temperature," *Corrosion Science*, vol. 50, May. 2008, pp. 1274-1282.

[2]   B.J. Skrifvars, M. Westén-Karlsson, M. Hupa, and K. Salmenoja, "Corrosion of super-heater steel materials under alkali salt deposits. Part 2: SEM analyses of different steel materials," *Corrosion Science*, vol. 52, Mar. 2010, pp. 1011-1019.

[3]   N.P. Padture, M. Gell, and E.H. Jordan, "Thermal barrier coatings for gas-turbine engine applications.," *Science (New York, N.Y.)*, vol. 296, Apr. 2002, pp. 280-4.

[4]   M. Kawaji, X.H. Shen, H. Tran, S. Esaki, and C. Dees, "Prediction of heat transfer in the kraft recovery boiler superheater region," *Tappi Journal*, 1995.

[5]   J.R. Kish, C. Reid, D.L. Singbeil, and R. Seguin, "Corrosion of High-Alloy Superheater Tubes in a Coastal Biomass Power Boiler," *CORROSION*, vol. 64, 2008, pp. 356-366.

[6]   "Steam table program based on the IAPWS industrial formulation 1997 (IAPWS-IF97)."

[7]   J.B. Kitto and S.C. Stultz, eds., *Steam-Its generation and use*, The Babcock and Wilcox Company, 2005.

[8]   R. Fox and A. McDonald, *Introduction to Fluid Mechanics*, John Wiley & Sons, 1998.

[9]   V. Gnielinski, "New equations for heat and mass transfer in turbulent pipe and channel flow," *International Chemical Engineering*, vol. 16, 1976, pp. 359-368.

[10]   S. Haaland, "Simple and explicit formulas for the friction factor in turbulent type flow," *Journal of Fluids Engineering*, pp. 89-90.

[11]   S. Churchill and M. Bernstein, "A correlating equation for forced convection from gases and liquids to a circular cylinder in cross flow," *Journal of Heat Transfer*, vol. 99, 1977, pp. 300-306.

[12] M. Theis, B. Skrifvars, M. Hupa, and H. Tran, "Fouling tendency of ash resulting from burning mixtures of biofuels. Part 1: Deposition rates," *Fuel*, vol. 85, May. 2006, pp. 1125-1130.

[13] M.N. Ojisik, *Heat Transfer - A Basic Approach*, 1985.

[14] P. Harvey, ed., "AISI Type 304," *Engineering Properties of Steel*, American Society for Metals, 1982, pp. 273-277.

[15] O. Altun, Y.E. Boke, A. Kalemtas, and T. Eskisehir, "Problems for determining the thermal conductivity of TBCs by laser-flash method," *Journal of Achievements in Materials and Manufacturing Engineering*, vol. 30, 2008, pp. 115-120.

[16] S.M. Meier and D.K. Gupta, "The Evolution of Thermal Barrier Coatings in Gas Turbine Engine Applications," *Journal of Engineering for Gas Turbines and Power*, vol. 116, 1994, p. 250.

[17] J. Wu, H.-bo Guo, L. Zhou, L. Wang, and S.-kai Gong, "Microstructure and Thermal Properties of Plasma Sprayed Thermal Barrier Coatings from Nanostructured YSZ," *Journal of Thermal Spray Technology*, vol. 19, Aug. 2010, pp. 1186-1194.

3 Preliminary Corrosion behaviour of YSZ environmental barrier coatings exposed to NaCl salt at 600°C

3.1 Introduction

Accumulation of deposits on superheater tubes in recovery boilers reduce the thermal efficiency of the boiler and may also cause corrosion problems. These deposits are derived from three different sources – carryover, fume and intermediate sized particles. Carryover particles are relatively large (0.01 to 3 mm) molten or partially molten smelt particles, and/or particles of partially burned black liquor solids entrained in the flue gas. Fume deposits are formed as a result of the condensation of vapors of sodium and potassium compounds in the flue gas. Smaller particles (1 to 100 µm) which are entrained in the flue gas are the intermediate sized particles (ISP) [1]. The following chapter aims to explore the effects of solid corrosives on yttria-stabilized zirconia (YSZ) coatings. This chapter documents the effects of NaCl salt on conventional yttria-stabilized zirconia (YSZ) and nanostructured YSZ coating samples. These samples were exposed to sodium chloride (NaCl) salt and air in a furnace at 600°C for 76 hours.

3.2 Experimental Procedure

Thermal Spraying

All samples consisted of a bond coat and a top coat. Ni-Cr-Al-Co-Y_2O_3 bond coat powder (Metco 461NS, Sulzer Metco, Inc., Westbury, NY, USA) was deposited using a plasma spray torch (3MBM ThermoSpray Gun, Sulzer Metco, Inc., Westbury, NY, USA). Conventional YSZ (Metco 204NS-G, Sulzer Metco, Inc., Westbury, NY, USA) and nanostructured YSZ (Nanox Powder S4007, Inframat Corporation, Farmington, CT, USA) were deposited as the top coats using the same plasma spray torch. The spray parameters for deposition of the bond coat and the top coat are shown in Table 1. A robot (HP20, Motoman, Inc., West Carrollton, OH, USA) operating at 400 mm/s was used to deposit the coatings.

Table 1: Plasma spraying parameters

Spray Parameter	Bond Coat (Ni-Cr-Al-Co-Y_2O_3)	Top Coat (YSZ)
Primary Gas	Argon	Argon
Secondary Gas	Hydrogen	Hydrogen
Ar flow rate	90 SCFH	90 SCFH
H_2 flow rate	20 SCFH	30 SCFH
Ar pressure	75 psig	75 psig
H_2 pressure	100 psig	100 psig
Carrier gas pressure	60 psig	60 psig
Carrier gas flow rate	14 SCFH	14 SCFH
Standoff distance	5.5 in	2.5 in
Current	500 A	500 A
Voltage	60 V	60 V

The size distribution of the Ni-Cr-Al-Co-Y_2O_3 powder was between 22 μm and 150 μm (-150+22 μm). The conventional and nanostructured YSZ powders were sieved with a Ro-Tap siever (RX-29-CAN, W.S. Tyler, Mentor, OH, USA) to obtain a size distribution of 20 to 63 μm (-63+20 μm) and 20 to 90 μm (-90+20 μm). All coatings were deposited onto Type 316 stainless steel substrates with dimensions of 25 mm x 20 mm x 2 mm. All substrates were grit blasted with #24 alumina grit before the bond coat was applied.

Corrosion Testing

Once all the samples were sprayed with the respective coatings, they were cleaned according to the following procedure before being introduced into the furnace.

- 2 minutes sonification in dilute Versaclean (Fisherbrand Versaclean, Thermo-Fisher Scientific, Fairlawn, NJ, USA).

- Warm tap water rinse.

- 2 minutes sonification in de-ionised water.

- Dip in clean, wet 95% ethanol (Ethyl Alcohol, Brenntag, Toronto, Ontario, CANADA).

- 2 minutes sonification in dry, filtered (anhydrous) ethanol (Ethyl Alcohol, Brenntag, Toronto, Ontario, CANADA).

- Coupons were placed in a stainless steel mesh and dried rapidly with hot air from a hair dryer.

The corrosion test comprised of two different tests, test A and test B. During test A, the samples were exposed to air only, in a furnace maintained at 600°C for 76 hours; while in test B, the samples were first coated with NaCl (Sodium Chloride ACS grade, Thermo-Fisher Scientific, Fairlawn, NJ, USA) salt and then kept in the furnace heated to 600°C for 76 hours. Each test consisted of 3 different kinds of samples: uncoated stainless steel substrates, stainless steel substrates with conventional YSZ top coats, and stainless steel substrates with nanostructured YSZ top coats. The coating thickness and the type of powder used for preparing the samples are shown in Table 2. The first letter in the sample name corresponds to the type of test and the second letter represents the different samples.

A thin layer of NaCl salt was coated on top of the YSZ-coated substrates for test B. For this purpose, a saturated NaCl solution in de-ionised water (360 g/litre) was prepared. This salt solution was then sprayed on the samples using an artist's air brush (Iwata HP-BC 1 Plus, Iwata Medea, Inc., Portland, OR, USA). The air pressure used was 20 psi and the stand-off distance − the distance between the brush and the sample − was 190 mm. While the solution was being sprayed, the substrates were maintained at a constant temperature of 130°C. This allowed the water from the solution to evaporate immediately, leaving a layer of solid salt on the coated sample. A jig was manufactured in order to keep the substrate perpendicular to the axis of the air brush. This assembly is shown in Fig. 1.

Table 2: Information about the samples used in Test A and Test B.

Sample	Test	Bond Coat Thickness (μm)	Top Coat Thickness (μm)	YSZ Powder Size (μm)	YSZ Powder Type
AA	A	(uncoated)	(uncoated)	-	-
AB	A	150	365	-90+20	Conventional
AC	A	150	365	-90+20	Nano-structured
BA	B	(uncoated)	(uncoated)	-	-
BB	B	150	275	-63+20	Conventional
BC	B	150	200	-63+20	Nano-structured
BD	B	150	365	-90+20	Conventional
BE	B	150	365	-90+20	Nano-structured

Figure 1: Salt spray apparatus

Once the samples were ready to be introduced into the furnace, they were arranged on a stub in an alumina crucible as shown in Figs. 2 and 3. These crucibles were placed on top of a D-shaped alumina support and then inserted into a mullite tube shown in Fig. 4. This mullite tube was then placed inside a 3-zone furnace. The furnace (Lindberg Model 55347, Lindberg/MPH, Riverside, MI, USA) was arranged horizontally as shown in Fig. 5. The samples were heated in the furnace for a continuous period of 76 hours in the presence of air (ISO Standard 85-73-1, Class 2), flowing at a rate of 200 standard cubic centimetres per minute (SCCM).

Figure 2: Alumina crucible and stub

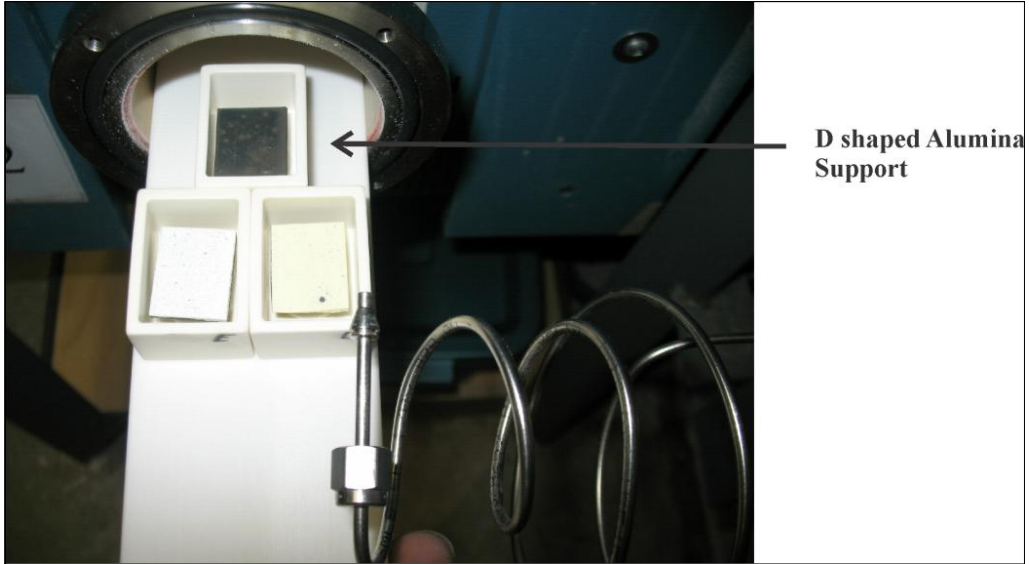**Figure 3:** Substrate sitting inside crucible

Figure 4: D-shaped alumina support
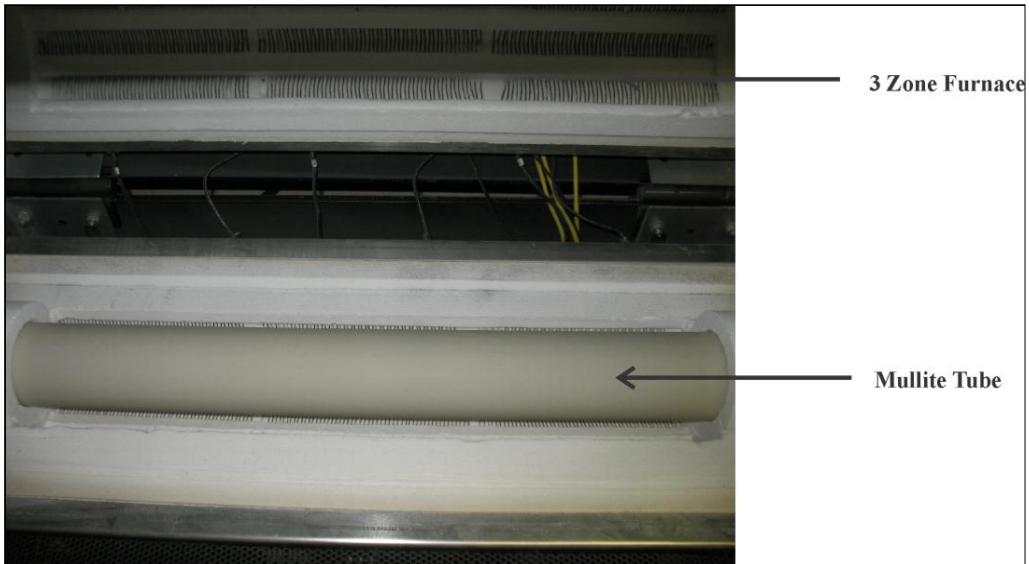
Figure 5: 3 Zone furnace and Mullite tube

Coating Analysis

After removing the samples from the furnace, they were cold-mounted in epoxy. Only the bottom half of the samples were mounted in epoxy, while the top half was left unmounted. The sample was then cut in half to separate the epoxy-mounted section from the bare, unmounted section. The bare section was analysed using X-ray diffraction (XRD) to identify the phases in the coating. The epoxy-mounted section was polished and prepared for analysis in a scanning electron microscope (SEM) (Zeiss EVO MA 15, Carl Zeiss SMT Inc., North America). All the cutting and polishing was done dry so as to avoid dissolution of the corrosion products in water or oil-based coolants. The operating parameters of the XRD system that were used to generate the patterns are shown in Table 3.

Table 3: Operating parameters for the XRD equipment

Instrument	RIGAKU rotating anode XRD system
Generator	RIGAKU RU-200B
Target(anode)	Copper
Power	40 kV, 110 mamps
Mode of operation	Reflective mode
Monochromator	Curved graphite
Mode	Continuous mode with a scan speed of 2 degrees per minute.
Divergence limiting slit (DS) = Soller slit (SS)	1°
Step Size	0.05°

3.3 Results and Discussion

SEM

Figure 6 shows SEM BSE (Backscattered electron) images of as sprayed conventional and nanostructured coating samples. It can be observed that the conventional YSZ coating shows more cracks as compared to the nanostructured YSZ coating.

Figure 7 shows BSE images of the cross-section of samples from Test A where they were exposed to $600^{o}C$ for 76 hrs in the presence of air. It was observed that there was no significant damage to the samples due to corrosion. It was possible to identify semi-molten nano-particles in the top coat of the nanostructured YSZ coating sample shown in Fig. 7c. Also, it can be seen that the number of cracks in the nano-structured top coat is less than in the conventional YSZ top coat. It has been hypothesized that these nano particles may act as crack arresters [2]. This could be a possible reason for fewer cracks in the nanostructured YSZ coating. No significant difference in cracking behaviour was found between the as sprayed samples and the samples from Test A.

Figure 8 shows BSE images of the cross sections of samples from Test B where they were exposed to $600^{o}C$ and NaCl salt for 76 hrs in the presence of medical grade air. The surface of the uncoated sample clearly appears to be corroded due to the NaCl salt. This can be confirmed from Fig. 9, which shows the images before and after exposure to the salt solution for corrosion testing. No such degradation is observed for the YSZ coated samples shown in Fig. 9. It can be seen from the images in Fig. 8 that the samples with the conventional YSZ top

coat, (Figs. 8b and 8d), show more cracks that are wider, as compared to the nano-structured YSZ top coat samples. The cracks in the conventional YSZ sample BD(Fig. 8d), which has a top coat thickness of about 365 microns, are more pronounced and wider than the cracks in the conventional YSZ sample BB(Fig. 8b), which has a thinner top coat (275 microns). This suggests that more stresses are induced in thicker coatings as compared to thinner ones, thereby leading to early coating failure. Again, no significant difference in cracking behaviour was found between the as sprayed samples and the samples from Test B.
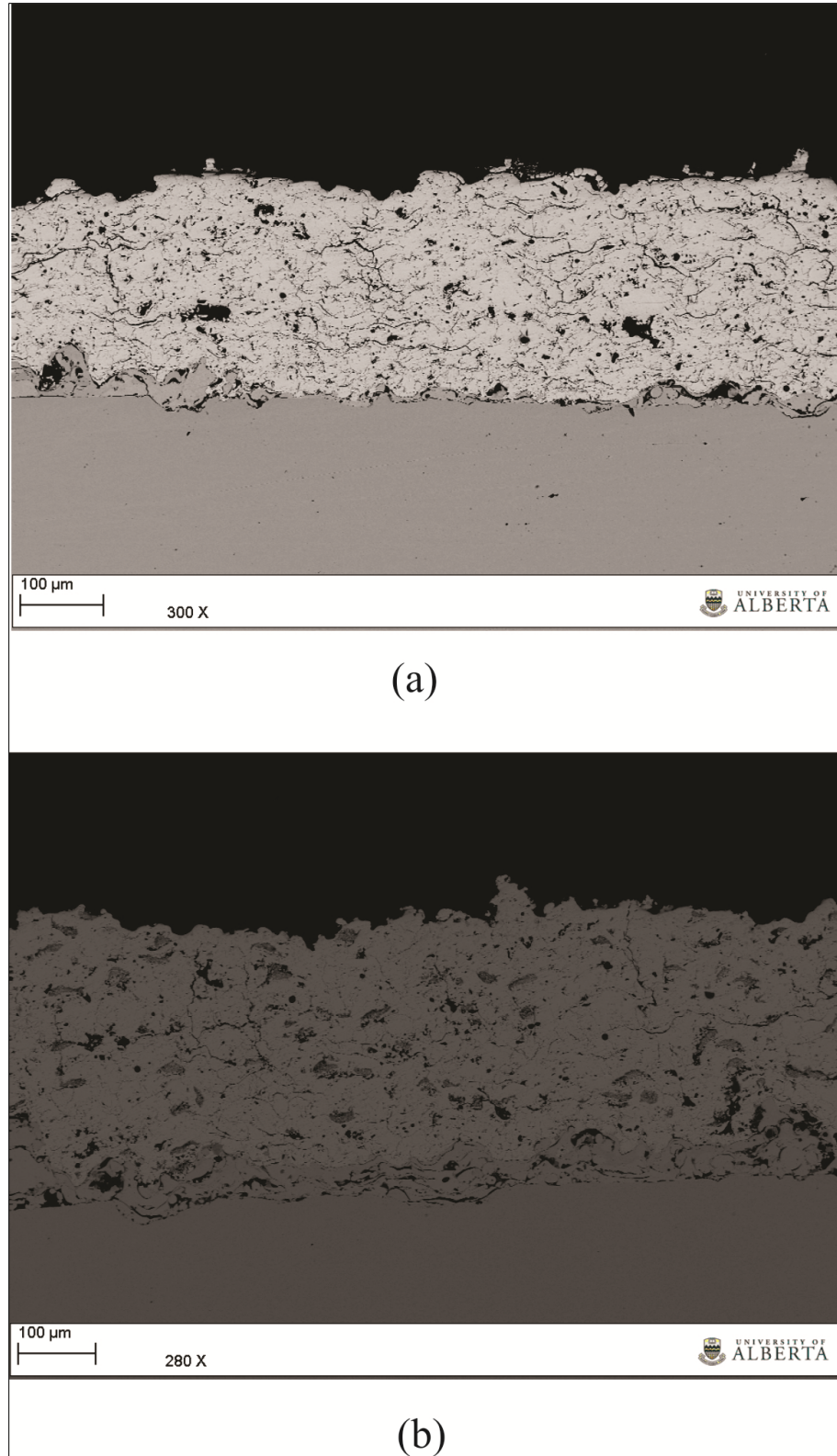
Figure 6: SEM BSE images of as sprayed (a) conventional YSZ and (b) nanostructured YSZ coatings
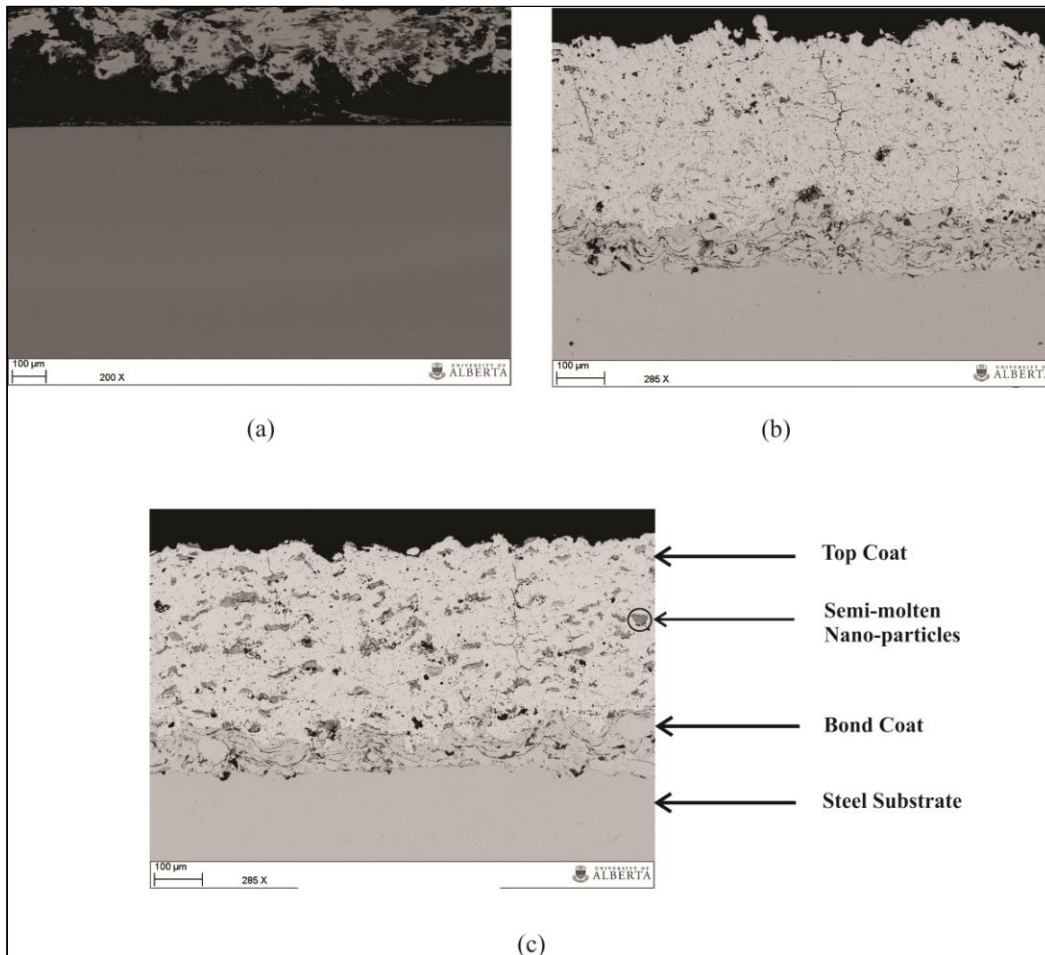
Figure 7: Cross sections of SEM BSE images for the (a) Bare steel (b) Conventional YSZ coating (c) Nanostructured YSZ coating samples from Test A (600°C, 76 hrs, air).
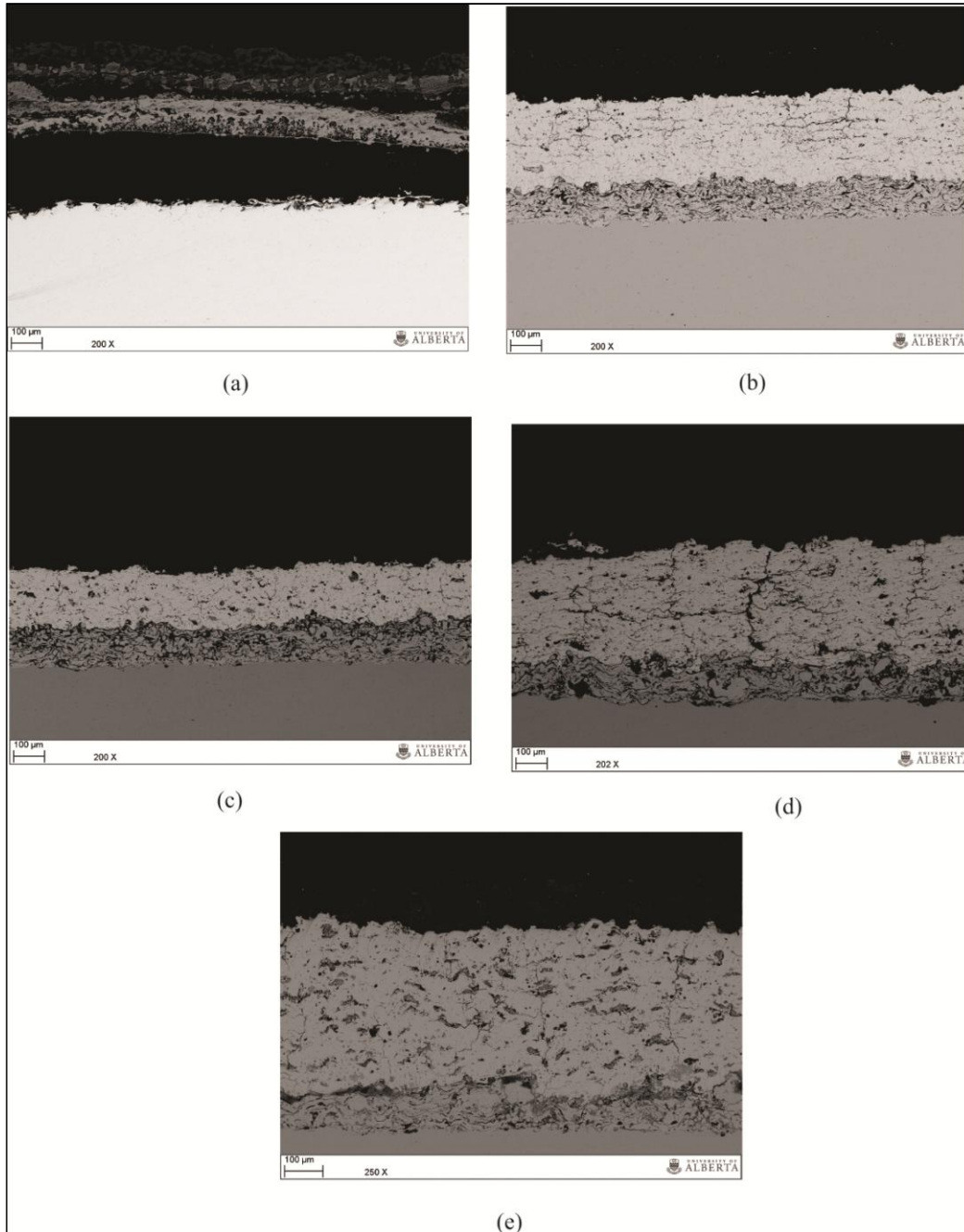
Figure 8: SEM BSE images of samples (a) BA(bare steel sample) (b) BB(conventional YSZ) (c) BC(nanostructured YSZ) (d) BD(conventional YSZ) and (e) BE(nanostructured YSZ) from Test B(600°C, 76 hrs, air, NaCl salt).

(a)   (b)
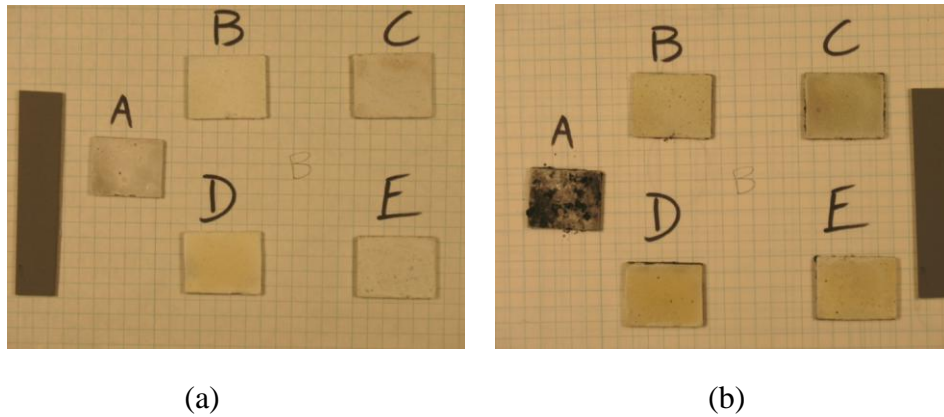
Figure 9: Images of samples from Test B (600°C, 76 hrs, air, NaCl salt) (a) before and (b) after corrosion testing

In order to determine if NaCl salt penetrated the YSZ coatings, an elemental mapping was done on the SEM images. EDS (Energy Dispersive Spectroscopy) images of conventional YSZ coating and nanostructured YSZ coating samples are shown in Figs. 10 and 11, respectively. In both these figures, it can be seen that Na and Cl species are concentrated on top of the YSZ layer, indicating that there is no penetration of the salts into the coating. This is also confirmed by observing the line spectrum shown in Fig. 12, for the nanostructured YSZ coating sample sample BE.
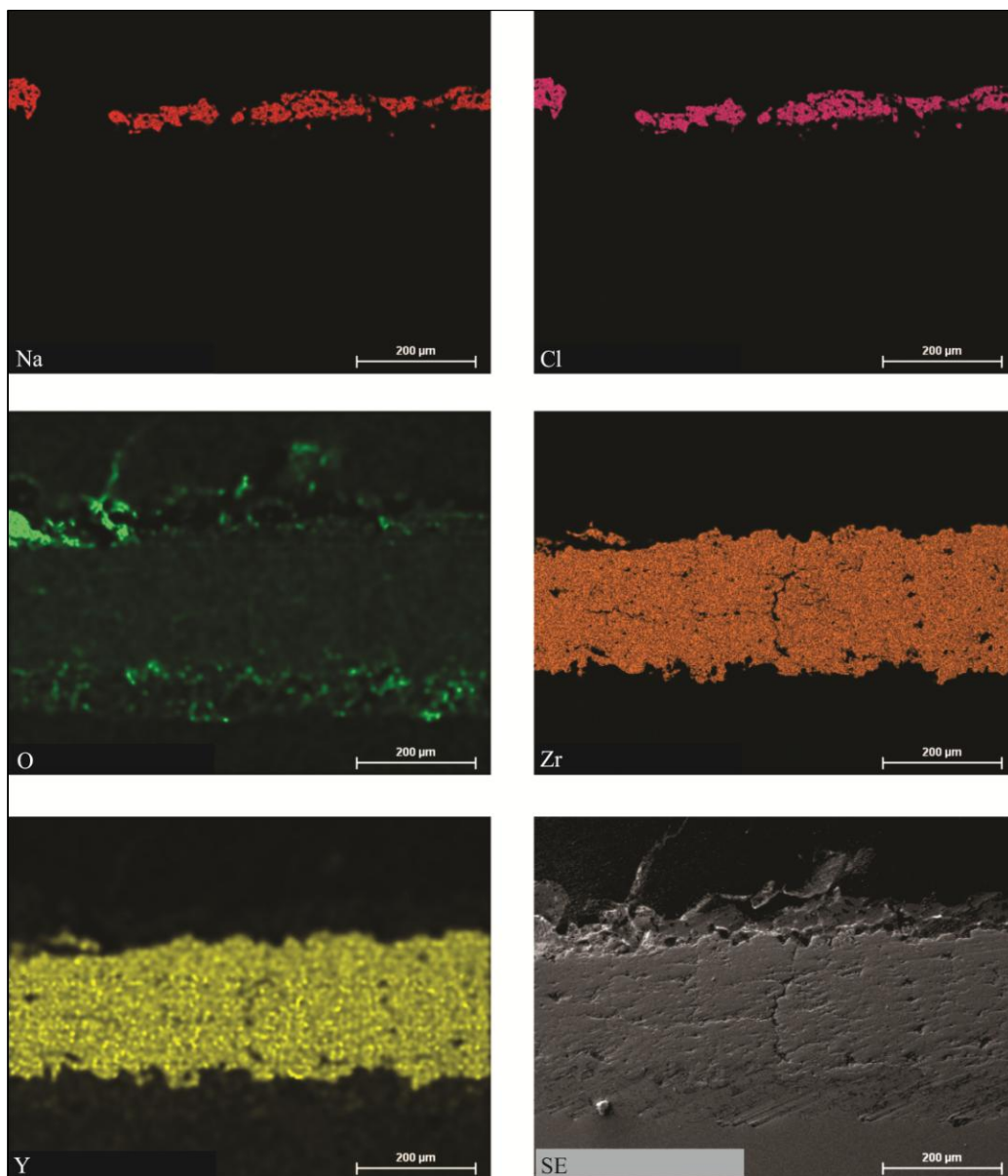
Figure 10: EDS images of conventional YSZ coating sample BD from Test B
$(600^{\circ}C, 76 \text{ hrs, air, NaCl salt.})$
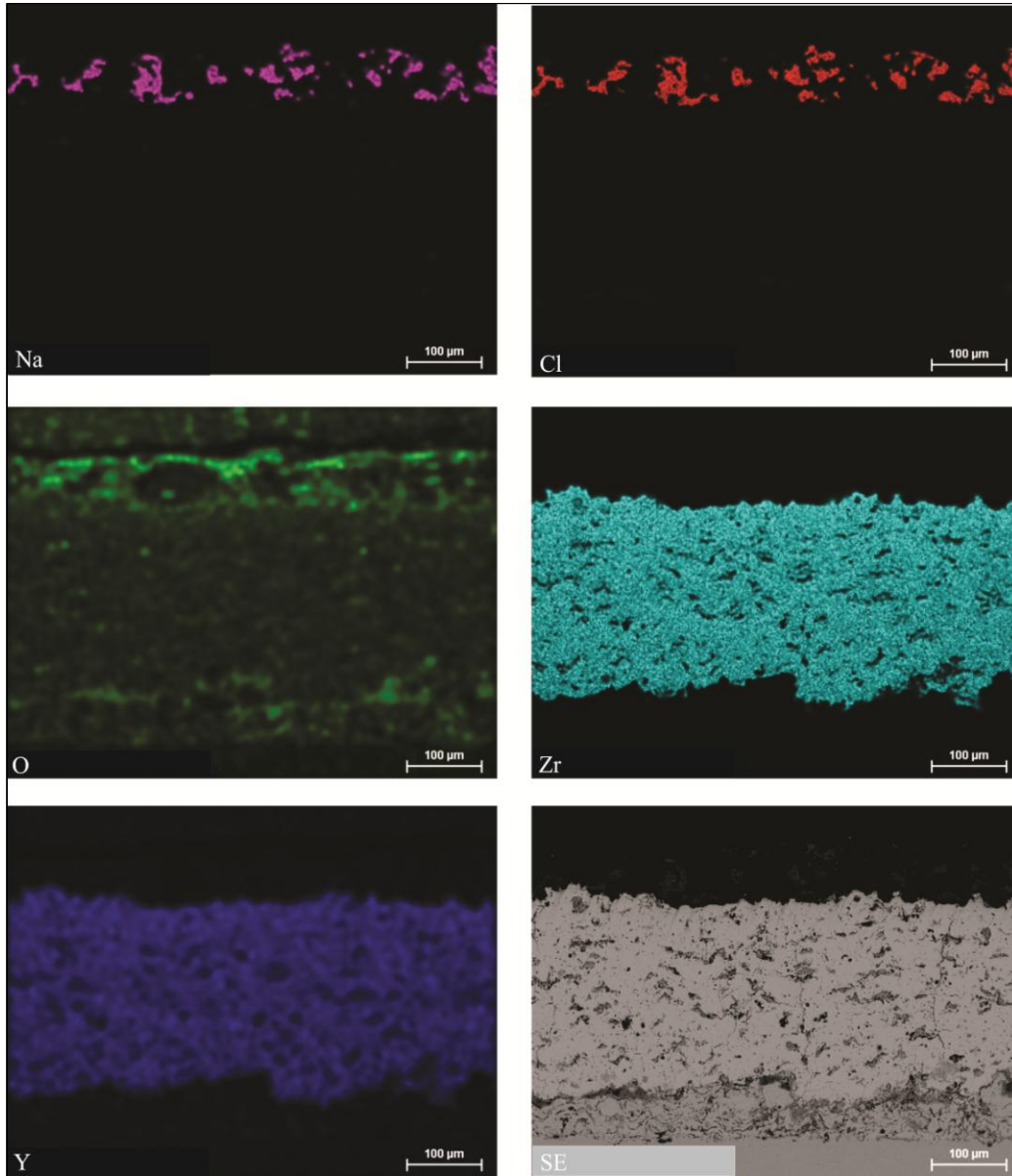
Figure 11: EDS images of nanostructured YSZ coating sample BE from Test B (600°C, 76 hrs, air, NaCl salt.)
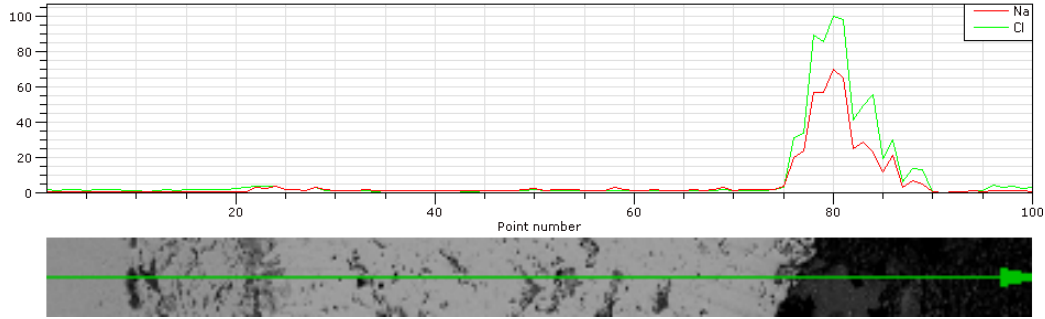
Figure 12: Line spectrum showing NaCl concentration on top of YSZ layer.

XRD

Metastable tetragonal phase (*t'*-phase) is the most desirable phase for the integrity of YSZ plasma-sprayed coatings [3]. A detailed discussion about this non transformable tetragonal phase has been provided in Chapter 1. The metastable tetragonal phase is identified by analysing the 72° to 75° region of the 2θ co-ordinate on the XRD pattern of YSZ. Figure 13 shows this region of the XRD pattern for the conventional YSZ powder and nanostructured YSZ powder, while Fig. 14 shows the same for as sprayed conventional and nanostructured YSZ coatings. The two peaks in this region can be associated with the metastable *t'* phase [3,4]. It is possible to see that the *t'* phase, which is present in the powders, has been retained in the as-sprayed coatings. XRD patterns of the YSZ samples used in test B are shown in Fig. 15. These patterns also showed the same peaks, indicating that the metastable phase was retained. This was expected since the exposure temperature was not high enough for the decomposition of the *t'* phase to the equilibrium *t* and *c* phases. Figure 15 shows the diffraction pattern for sample BB (conventional YSZ coating) and sample BE (nano-structured YSZ coating). NaCl peak can be clearly seen in the XRD patterns.
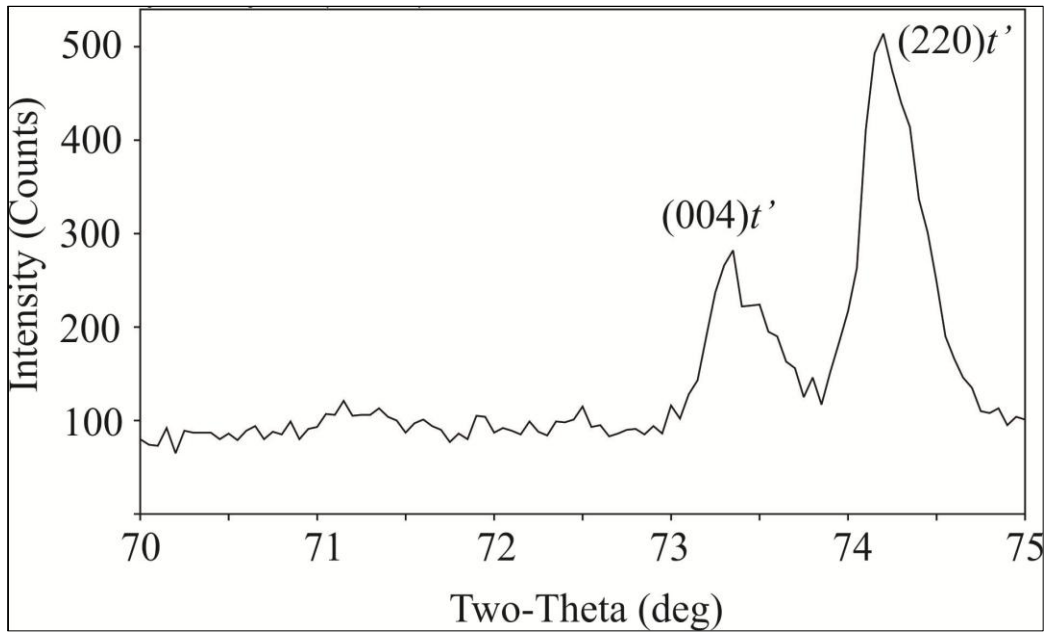
(a)
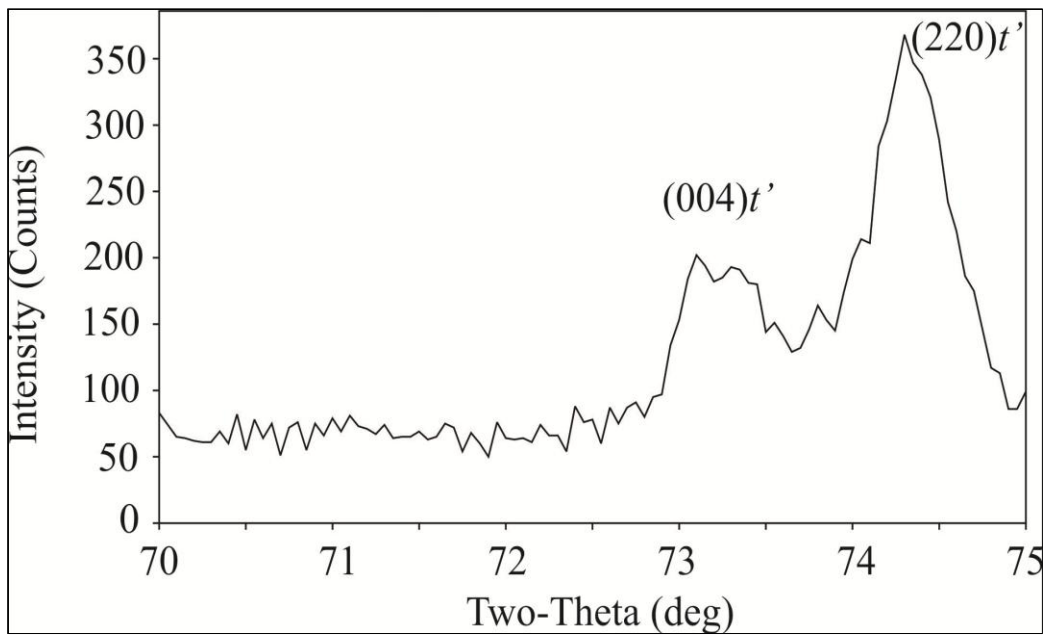
(b)

Figure 13: XRD pattern of (a) conventional (b) nano-structured YSZ powder

(a)
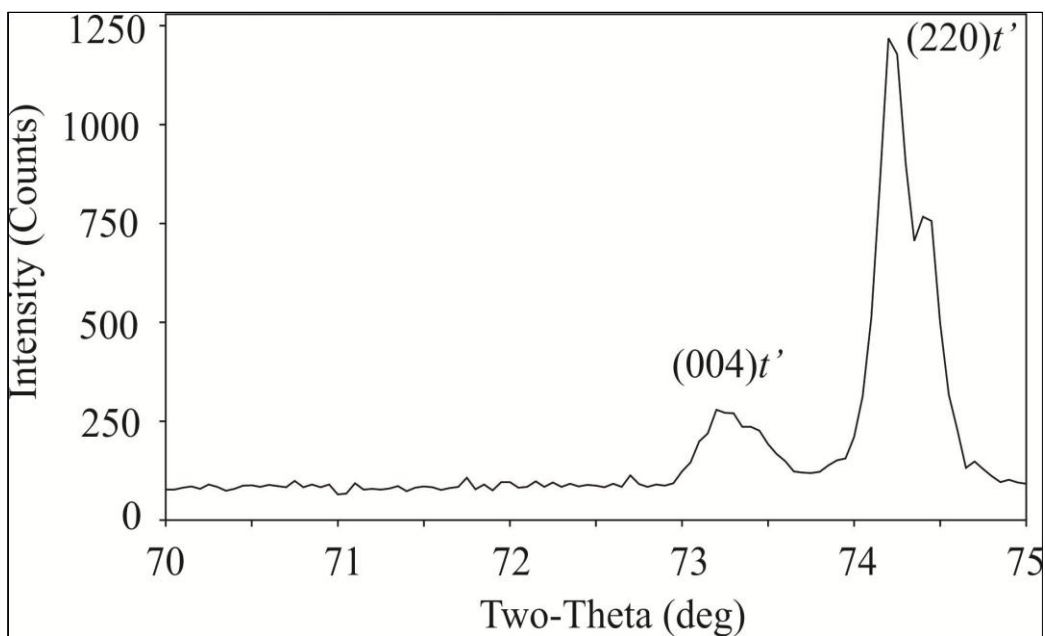
(b)

Figure 14: XRD pattern of as-sprayed (a) conventional (b) nano-structured YSZ coatings
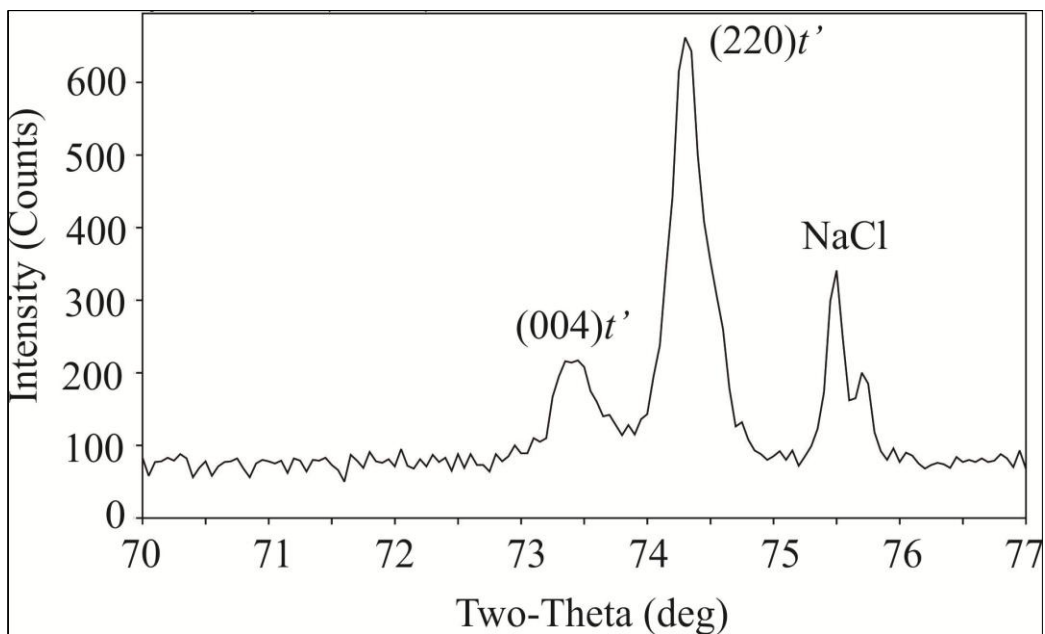
(a)
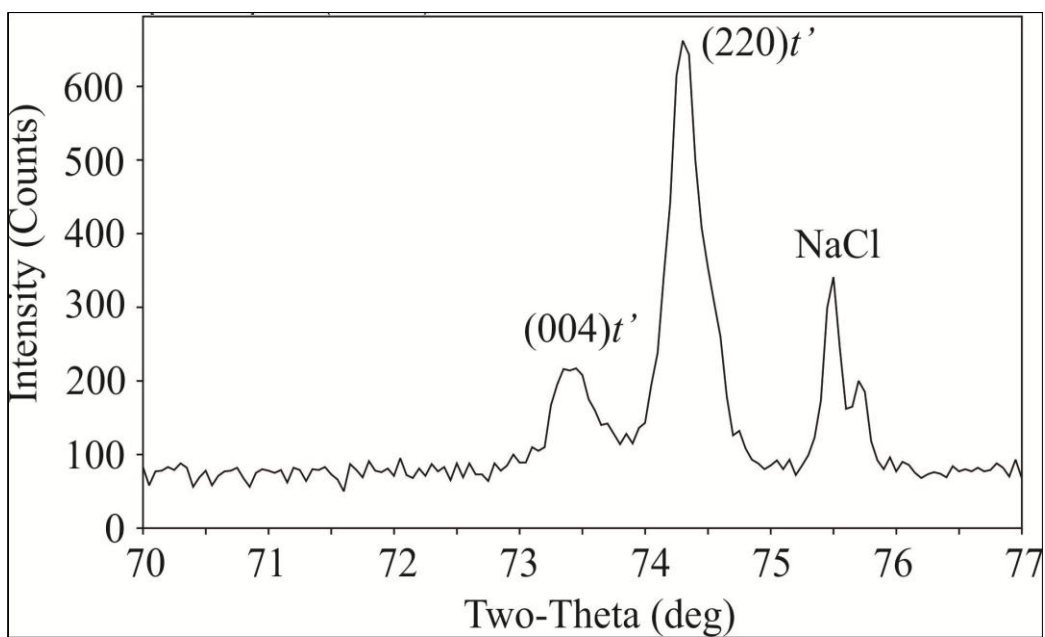
(b)

Figure 15: XRD pattern of samples (a) BB (conventional YSZ) (b) BE (nanostructured YSZ) from Test B (600$^{\text{o}}$C, 76 hrs, air, NaCl salt).

3.4 **Conclusion**

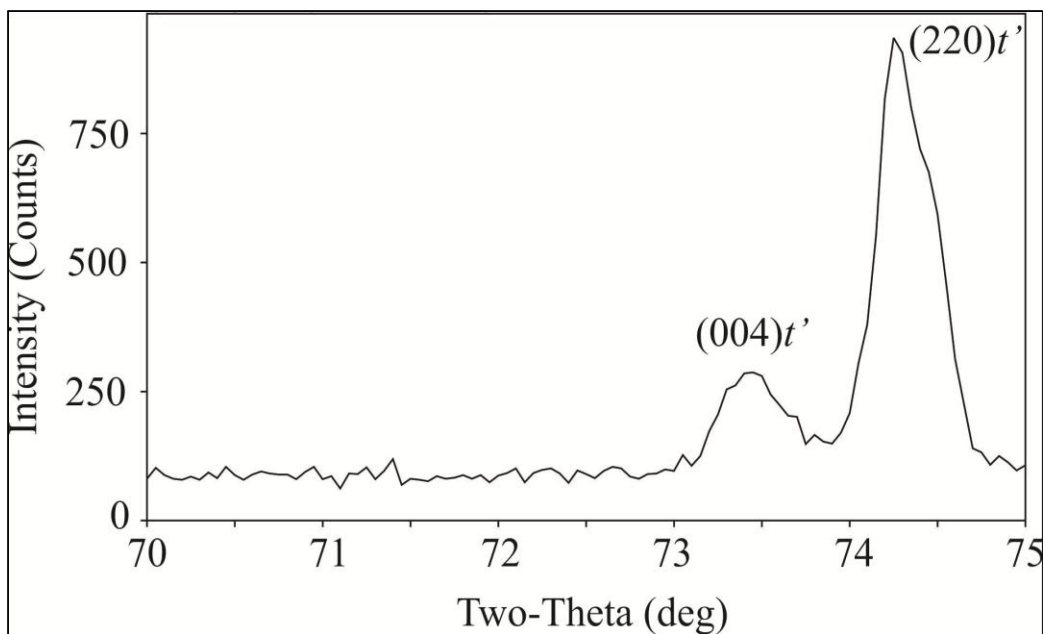The air plasma sprayed conventional YSZ and nanostructured YSZ samples were tested in a furnace maintained at 600^oC. A layer of NaCl salt was applied on top of the samples to corrode them. No significant difference in cracking behaviour was observed between the as sprayed samples and the coupons exposed to corrosion tests. However, it was found that the nanostructured YSZ coating exhibited fewer and narrower cracks as compared to its conventional counterpart. Semi-molten nano particles embedded in the microstructure of the nano based YSZ coating. These nano particles might have acted as crack arresters, thereby reducing the number of cracks in the coating. It was also found that more stresses are induced in a thicker ceramic coating as compared to a thinner one, possibly due to the large thermal expansion mismatch between the steel substrate and the ceramic coat. As a result, more cracks were found in the thicker coat as compared to the thinner one.

XRD analysis on the samples showed the presence of the non transformable tetragonal phase. This phase is the most desirable phase for YSZ coatings. Retention of this phase in the coating was expected since the exposure temperature was not high enough for the decomposition of this phase.

3.5 **References**

[1]   H.N. Tran, "Recovery Boiler Fireside Deposits And Plugging," *Tappi Kraft Recovery Short Course*, 2000.

[2]   R.S. Lima and B.R. Marple, "Thermal Spray Coatings Engineered from Nanostructured Ceramic Agglomerated Powders for Structural, Thermal Barrier and Biomedical Applications: A Review," *Journal of Thermal Spray Technology*, vol. 16, Mar. 2007, pp. 40-63.

[3]   K. Muraleedharan, J. Subrahmanyam, and S.B. Bhaduri, "Identification of t'Phase in ZrO_2-7.5 wt% Y_2O_3 Thermal-Barrier Coatings," *Journal of the American Ceramic Society*, vol. 71, 1988, pp. 226-227.

[4]   G. Witz, V. Shklover, W. Steurer, S. Bachegowda, and H.-P. Bossmann, "Phase Evolution in Yttria-Stabilized Zirconia Thermal Barrier Coatings Studied by Rietveld Refinement of X-Ray Powder Diffraction Patterns," *Journal of the American Ceramic Society*, vol. 90, Sep. 2007, pp. 2935-2940.

4 Resistance of nanostructured environmental barrier coatings to molten salt and high-temperature boiler flue gases

4.1 Introduction

Black liquor is a well known by-product of the Kraft process. Given that it has a thermal energy content of about $12.55 - 14.644$ MJ/mol, it is used as fuel in recovery boilers [1]. Smelt produced during the reaction accumulates on the bottom of the boiler and on superheater tube surfaces. It mainly consists of Na_2S and Na_2CO_3. Na_2SO_4 is formed on the superheater tubes due to the oxidizing environment present in the boiler [1]. Formation of such corrosive species on superheater tubes causes severe problems and the boiler has to be shut down for expensive maintenance and to replace severely corroded tubes.

Yttria-stabilized zirconia (YSZ) coatings fabricated from fused-and-crushed conventional powders have been shown to provide corrosion protection when used as thermal barrier coatings (TBC) on high-temperature jet engine blades [2] . Thermal barrier coating systems are currently fabricated with a metallic bond coat (e.g. NiCoCrAlY), deposited directly on the metal substrate, and a YSZ-based top coat (typically 8 wt% Y_2O_3-ZrO_2). Nanostructured YSZ is a recently engineered material, developed as an alternative to conventional fused-and-crushed YSZ used as thermal barrier coatings in gas turbines [3]. Nanostructured agglomerated particles, embedded in the microstructure of these coatings, have

improved the crack resistance and toughness of the coatings [4]. While these TBC's have been applied to corrosive gas environments in high-temperature jet engines, limited studies have been conducted on their performance in recovery boiler environments.

The present study examines the behavior of conventional and nanostructured YSZ coatings in the presence of molten salts and high-temperature boiler flue gases.

4.2 **Experimental method**

Thermal Spraying

The samples consisted of a bond coat and a top coat. Ni-Cr-Al-Co-Y_2O_3 bond coat powder (Metco 461NS, Sulzer Metco, Inc., Westbury, NY, USA) was deposited using a plasma spray torch (3MBM ThermoSpray Gun, Sulzer Metco, Inc., Westbury, NY, USA). Conventional YSZ (Metco 204NS-G, Sulzer Metco, Inc., Westbury, NY, USA) and nanostructured YSZ (Nanox Powder S4007, Inframat Corporation, Farmington, CT, USA) were deposited as the top coats using the same plasma spray torch. The spray parameters for deposition of the bond coat and the top coat are shown in Table 1. A robot (HP20, Motoman, Inc., West Carrollton, OH, USA) operating at 400 mm/s was used to deposit the coatings.

The size distribution of the Ni-Cr-Al-Co-Y_2O_3 powder was between 22 μm and 150 μm (-150+22 μm). The conventional and nanostructured YSZ powders were sieved with a Ro-Tap siever (RX-29-CAN, W.S. Tyler, Mentor, OH, USA) to obtain a size distribution of 20 to 90 μm (-90+20 μm). All coatings were

Table 1: Plasma spraying parameters

Spray Parameter	Bond Coat (Ni-Cr-Al-Co-Y$_2$O$_3$)	Top Coat (YSZ)
Primary Gas	Argon	Argon
Secondary Gas	Hydrogen	Hydrogen
Ar flow rate	90 SCFH	90 SCFH
H$_2$ flow rate	20 SCFH	30 SCFH
Ar pressure	75 psig	75 psig
H$_2$ pressure	100 psig	100 psig
Carrier gas pressure	60 psig	60 psig
Carrier gas flow rate	14 SCFH	14 SCFH
Standoff distance	5.5 in	2.5 in
Current	500 A	500 A
Voltage	60 V	60 V

deposited onto Type 309 stainless steel substrates with dimensions of 25 mm x 20 mm x 2 mm. All substrates were grit blasted with #24 alumina grit before the bond coat was applied.

In addition to the YSZ coated samples, Type 309 stainless steel samples were also included in the test to compare the extent of corrosion.

Corrosion Tests

Once all the samples were sprayed with the respective coatings, they were sonicated and cleaned using the following procedure:

- 2 minutes sonification in dilute Versaclean (Fisherbrand Versaclean, Thermo-Fisher Scientific, Fairlawn, NJ, USA).

- Warm tap water rinse.

- 2 minutes sonification in de-ionised water.

- Dip in clean, wet 95% ethanol (Ethyl Alcohol, Brenntag, Toronto, Ontario, CANADA).

- 2 minutes sonification in dry, filtered (anhydrous) ethanol (Ethyl Alcohol, Brenntag, Toronto, Ontario, CANADA).

- Coupons were placed in a stainless steel mesh and dried rapidly with hot air from a hair dryer.

The corrosion experiment consisted of 3 different tests with different corrosion parameters as follows.

- Test A: Exposure to salt vapors and flue gases.

- Test B: Exposure to molten salt and air.

- Test C: Exposure to molten salt and flue gases.

The experiment involved setting up and calibrating various equipments, including furnaces and mass flow controllers. Given below is a brief description of the methods employed to set up the experimental apparatus.

1. Salt Application

   A synthetic salt mixture (10.2 wt.% KCl, 11.5 wt.% Na_2CO_3, 73.9 wt.% Na_2SO_4, 4.4 wt.% K_2SO_4) was used as the corroding agent. It was first dissolved in distilled water and a saturated solution was formed(192 g/litre). This salt solution was then sprayed on to a few test samples using

an artist's air brush (Iwata HP-BC 1 Plus, Iwata Medea, Inc., Portland, OR, USA). The air pressure used was 20 psig and the stand-off distance – the distance between the brush and the sample – was fixed at 190 mm. The apparatus is shown in Fig. 1. While the solution was being sprayed, the substrates were maintained at a temperature around $130^{\circ}C$. This allowed the water from the solution to evaporate immediately, leaving a layer of solid salt on the coated sample. A jig was manufactured in order to keep the substrate perpendicular to the axis of the air brush. The salt was scraped off from the test sample and sent for a differential thermal analysis (DTA). The DTA analysis confirmed that the salt had a single first melting point of around $520^{\circ}C$. The first melting point is the temperature at which the material first begins to melt and below which there is no liquid phase in the salt [5].

Figure 1: Salt spray apparatus

Once this was confirmed, the same procedure was used to coat salt on samples in Test B and Test C before introducing them into the furnace. In order to ensure that all samples had approximately the same amount of salt, they were weighed before and after application of the salt coating. On average, each sample had approximately 18.61 ± 2.45 mg/cm^2 ($n = 10$) of salt on their surface.

2. Furnace setup

All three tests were conducted simultaneously in three different horizontal furnaces (Lindberg Model 55347, Lindberg/MPH, Riverside, MI, USA) maintained at 600ºC. Figure 2 shows one end of the horizontal furnace. All samples were arranged on a stub in an alumina crucible as shown in Figs. 3 and 4.

Figure 2: Front end of horizontal furnace.

Figure 3: Alumina crucible and stub

Figure 4: Substrate sitting inside crucible

These crucibles were placed on top of a D-shaped alumina support and then inserted into a 48 inch mullite tube shown in Fig. 5. This mullite tube was then placed in the 3-zone furnace as shown in Fig. 6. The ID of the mullite tube used was 72 mm. All furnaces were arranged horizontally. Figure 6 shows the 3 zones inside the furnace. At the furnace controller, the input was fed in such a way that a 12 inch section at the centre of the mullite tube was maintained at 600 ± 3ºC. The input to the furnace controller consisted of 3 different parameters corresponding to the 3 zones inside the furnace. These 3 parameters In, Centre and Out. The desired furnace temperature was specified to the central zone. Variation from this temperature was fed into the In and Out parameters. For example, suppose the input parameters to the furnace controller were as follows:
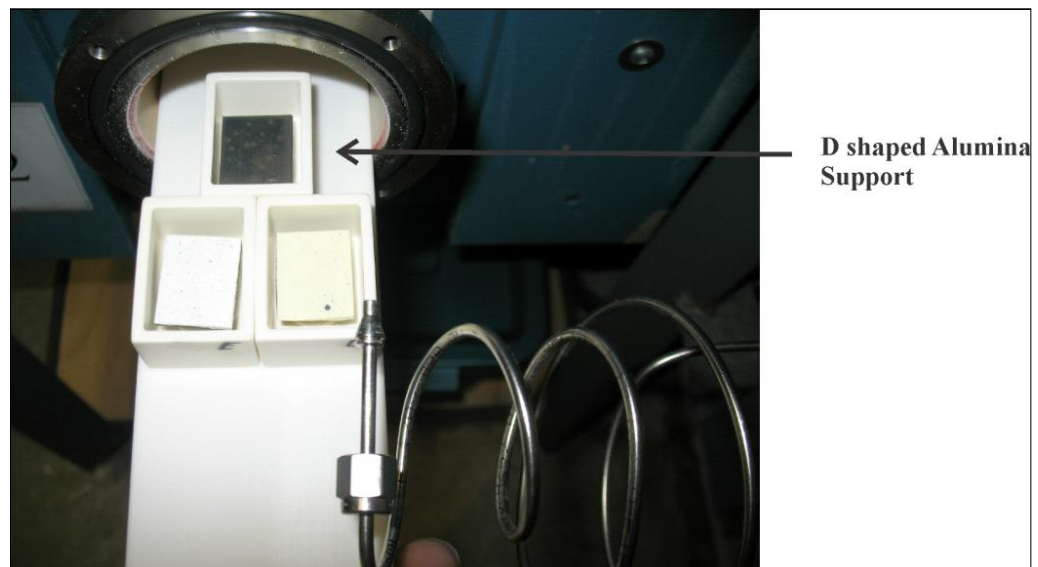

D shaped Alumina Support

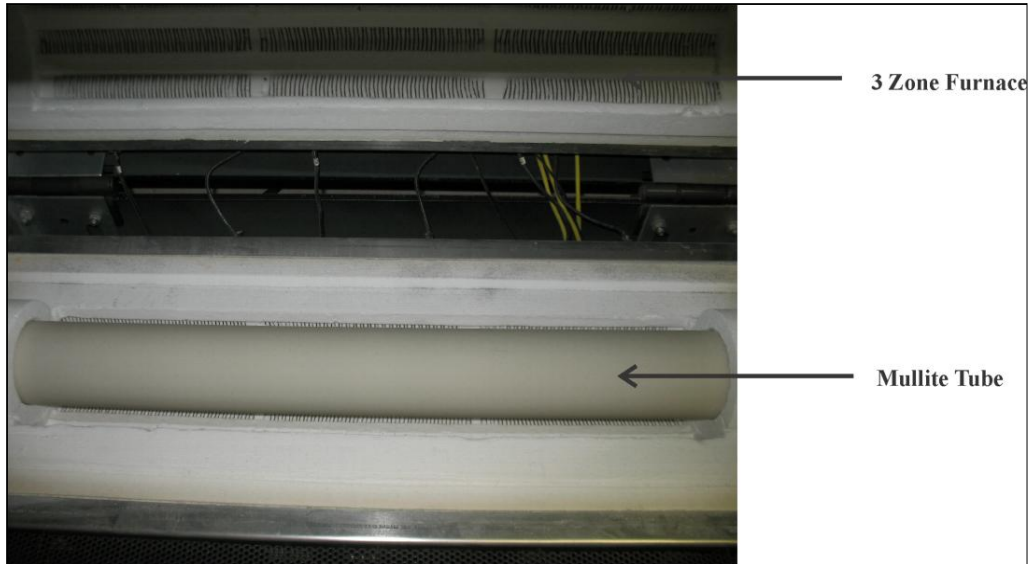**Figure 5:** D-shaped alumina support

Figure 6: 3 Zone furnace and Mullite tube

In: + 2.3   Centre: 598   Out: +2.3

By giving the above input, the central zone tried to maintain the temperature at 598 ºC while the inner zone (gases entering) was maintained at 598 + 2.3 = 600.3ºC and the outer zone (gases leaving) was maintained at 598 + 2.3 = 600.3ºC. With these settings, we measured the temperature every 2 inches (50.8mm) across the centre for the entire 12 inches (304.8 mm) of the furnace and documented it as shown in Fig. 7. From this figure, we found that the temperatures at the centre and at the -6 (152.4 mm) positions were greater than the targeted ± 3ºC variation from 600ºC (data circled in red). Hence, we changed our input parameters until the targeted 600 ± 3ºC temperature range was achieved.
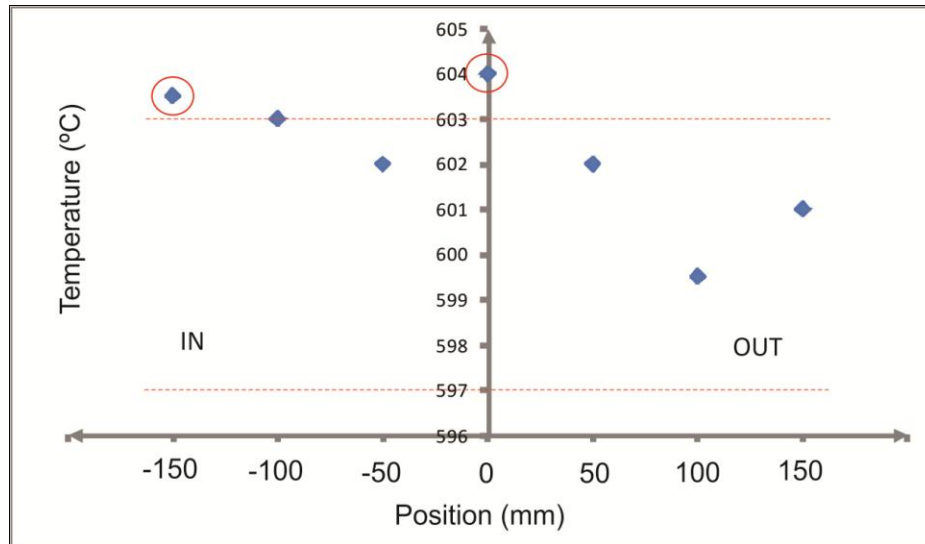
Figure 7: Furnace tuning data.

3. Mass flow controller setup

The simulated boiler flue gas used in the experiment consisted of 5% O_2, 10% CO_2, 20% H_2O, balance N_2, and the total flow was maintained at 200 standard cubic centimeters per minute (SCCM). The volume flow rate of air in test B was also maintained at 200 SCCM. Mass flow controllers (MFC) ranging from 20 SCCM to 1000 SCCM regulated flow of all gases. A 4-channel monitor (MKS Type 247C, Andover, MA, USA) was used to set the gas flow rate values and each channel corresponds to the flow of one gas. Every channel of the 4 channel monitor had its own scale factor setting. The scale factor setting was calculated by multiplying the gas correction factor and the gauge factor. The gas correction factor was different for different gases and was provided by the manufacturer of the mass flow controller. The gauge factor was also different for different

MFC's depending on their maximum flow capacity and was also provided by the manufacturer. A bubble flow meter was employed to confirm the flow rate of gases through the furnace. It consisted of a glass pipette with a rubber bulb at the bottom filled with soapy water. The pipette had markings of 0, 1, 10 and 100 ml. Just above the rubber bulb and below the 0 ml mark was an opening which was connected to the gas line for the gas whose flow was being calibrated. The gas was then switched on to produce flow through the pipette. As the rubber bulb (filled with soapy water) was pressed, water rose up and a bubble was formed. The bubble rose in the pipette pushed by the flowing gas. Time taken by the bubble to cover a fixed volume, say 90 ml, was measured using a stopwatch. From this information, the actual volume flow rate of the gas could be calculated. If this flow was not within permissible allowance limits, the scale factor was tuned slightly and the flow was checked again.

4. Water pump setup.

Out of 200 SCCM total gas flow thorough the furnace, 20% consisted of H_2O. Thus, 40 SCCM H_2O had to be introduced into the furnace. A peristaltic pump (IPC High Precision multichannel dispenser, ISMATEC SA, Glattbrugg, Switzerland) was used for this purpose. The total amount of water required for 2 furnaces for a total period of 168 hours was calculated as follows:

Total number of moles in 40 SCCM water is given by

$$\frac{40\,\text{SCCM}}{22.4\,\text{L}} = \frac{40\,\text{SCCM}}{22.4 \times 1000\,\text{SCCM}} = 0.00178\,\text{mol}$$

1 mole of water weighs 18.01528 g and 1 g of water occupies 1 ml volume. Thus, 0.00178 moles will occupy

$$0.00178\text{mol} \times \frac{18.01528\text{g}}{\text{mol}} \times \frac{1\text{ml}}{\text{g}} = 0.032\text{ml}$$

Therefore, 0.032 ml of water needs to flow through the furnace every minute. For 168 hours, we will require

$$\frac{0.032\text{ml}}{\text{min}} \times \frac{60\,\text{min}}{\text{hr}} \times 168\text{hrs} = 322.56\text{ml}$$

Two furnaces require 322.56×2 = 645.12 ml of H_2O.

Coating Analysis

After the test, the samples were removed from the furnace and mounted in epoxy. As the samples were porous, the pores were filled with epoxy by conducting vacuum impregnation. It was important to ensure that the corrosion scales and salts were present in the coating while analyzing the cross section in a scanning electron microscope (SEM). This would allow us to gauge the extent of salt penetration into the coating. Hence, all sample preparation processes such as cutting, grinding and polishing were done dry and without the use of any coolant or lubricant. The samples were cut in half by using a metal bonded diamond blade. In order to ensure reproducibility of the cut on all samples, an automated cutting machine (Accutom-50, Struers A/S, Ballerup, Denmark) was used. SiC grit paper was then used to grind the samples. Grinding was started with a 400 grit paper and then gradually increased to 1200 grit. After grinding, fine alumina

powder on napped cloth was used for final polishing. Energy dispersive spectroscopy (EDS) was used to confirm the composition of the salt crystals.

4.3 **Results**

Test A

This test involved exposing the coupons to flue gases and salt vapors, only. Hence, the coupons were not sprayed manually with a salt solution. Salt vapors in this case were contaminants originating from other test samples. Figure 8 shows an SEM image of the cross section of Type 309 steel used in this test. It can be clearly seen that the corrosion scale has spalled off the bare steel sample. Figure 9a shows an SEM image of the cross section of the conventional YSZ-based EBC. Salt crystals, shown by white arrows, can be seen in the bond coat of this coating. This is confirmed by the EDS spectrum presented in Fig. 9b. The EDS spectrum shows the presence of elements such as Na and K, which were present in the corroding salt. Cross-sectional images of the nano-based YSZ EBC coating used in this test are shown in Fig. 10. No salt crystals were found in the cross section of the nano-based EBC coatings.
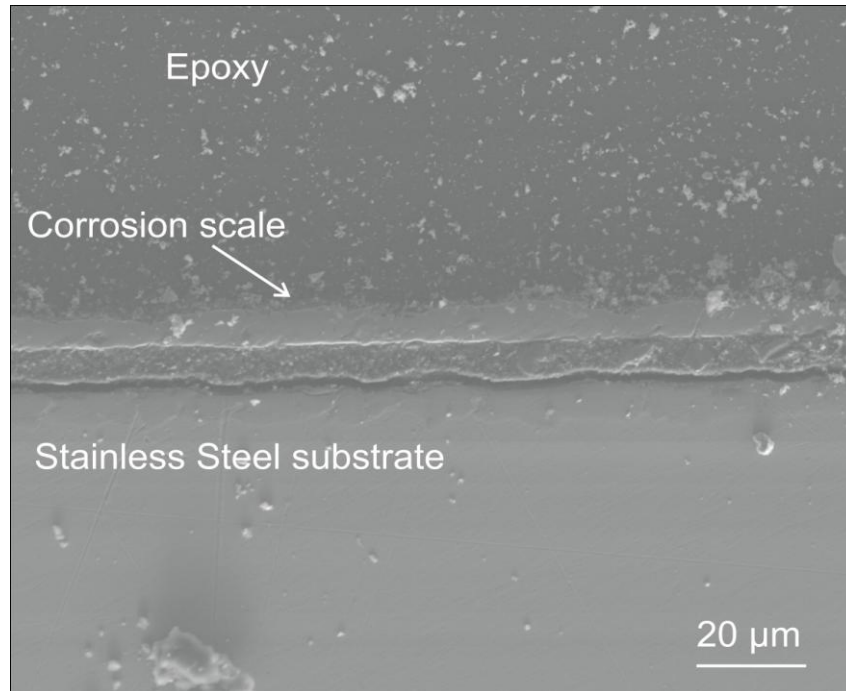
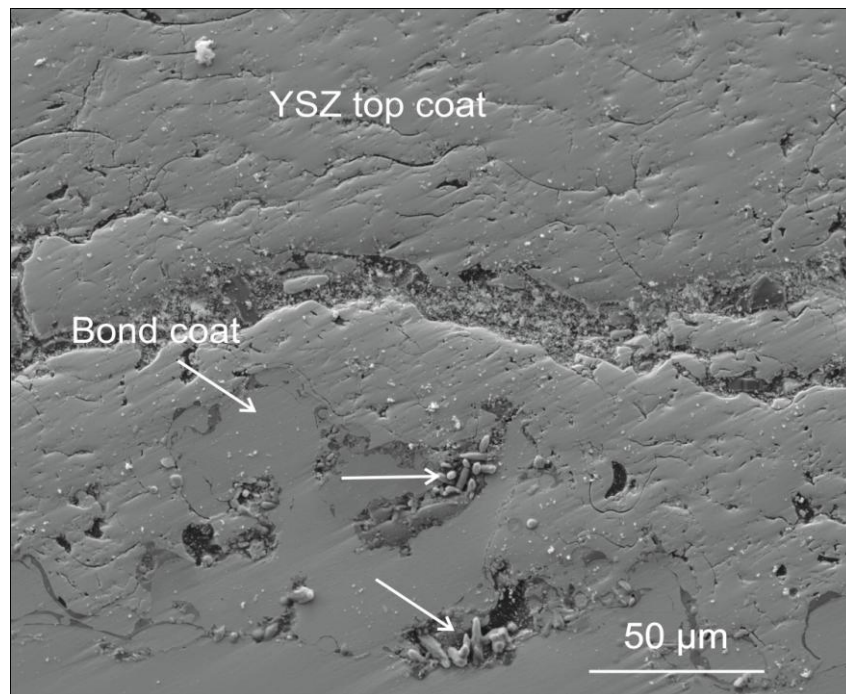**Figure 8:** SEM image of cross section of Type 309 steel

Figure 9(a): SEM image of cross section of conventional YSZ top coating.
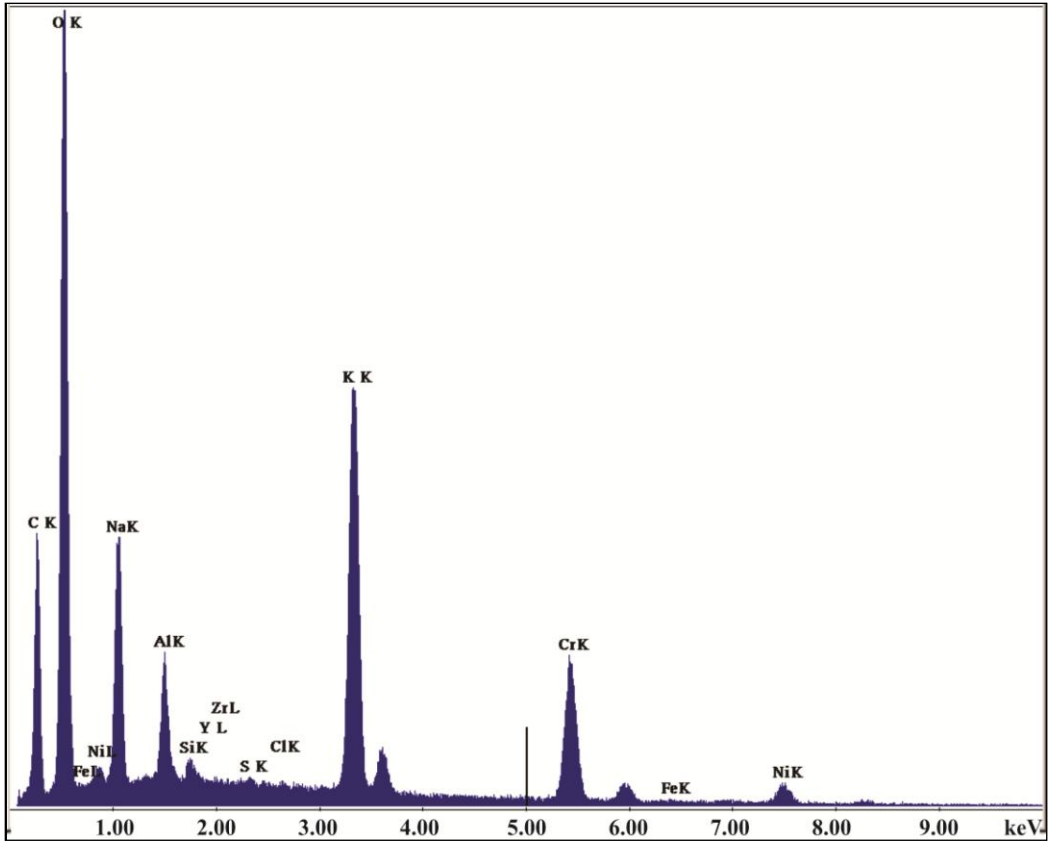Arrows point to salt crystals.

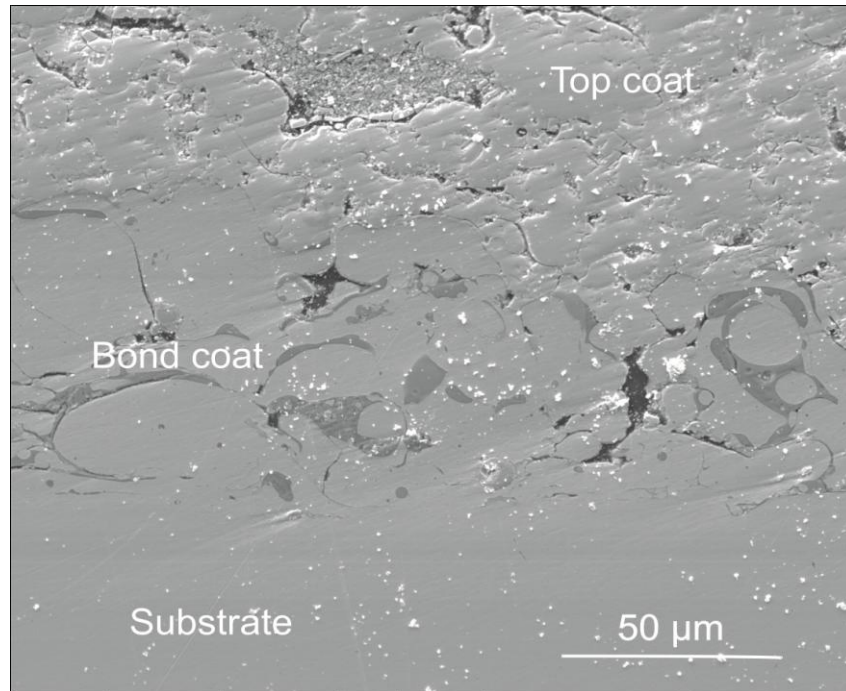**Figure 9(b):** EDS spectrum of crystals in the conventional YSZ top coat

Figure 10: SEM image of cross section of nanostructured YSZ coating

Test B

Test B involved exposing the samples to molten salts in the presence of medical grade air flowing at 200 SCCM. As shown in Fig. 11, the corrosion scale has spalled off the bare steel sample, similar to that shown in Fig. 8. Salt crystals can be seen at the top of the image and are shown by the white arrows. The substrate below the scale also appears to have been attacked.

Figure 12a shows the cross section of a conventional YSZ top coat. Salt crystals can be seen in cracks present in the top coat and are shown by white arrows. A spot scan was performed on the salt crystals pointed by the white arrow on the right side of the image. The EDS spectrum resulting from this scan is shown in Fig. 12b. It confirms the presence of Na, S, K, O and a little Cl. Figure

12c shows a high magnification image of a salt crystal. This crystal was found at the interface between the steel substrate and the bond coat over which the conventional YSZ based top coat was deposited. EDS spectrum of this image is shown in Fig. 12d. Constituent elements present in the corroding salt like Na, K, S and Cl could be found in this spectrum which indicates that the salt penetrated into the conventional EBC till it reached the substrate.

A typical cross section of the nanostructured YSZ-based EBC coating is shown in Fig. 13a. Although salt crystals were found in the YSZ top coat, none were found in the bond coat or near the steel substrate of this sample. The white arrow in the image points to the salt crystals. Unlike the conventional YSZ top coat, where salt was found in cracks in the coating (see Fig. 12a), it tended to crystallize in zones of semi-molten nanoparticles in the nano based YSZ top coat. This is evident from Fig. 13b, which is a high-magnification SEM image of the cross section of a nanostructured YSZ top coating. The presence of the semi-molten nanoparticles also confirm that the coating will have nanostructured characteristics and a bimodal microstructure. Figure 13c is an EDS spectrum of the crystal in Fig. 13b and it confirms the presence of elements like Na, S, K and some Cl, which were present in the corroding salt.
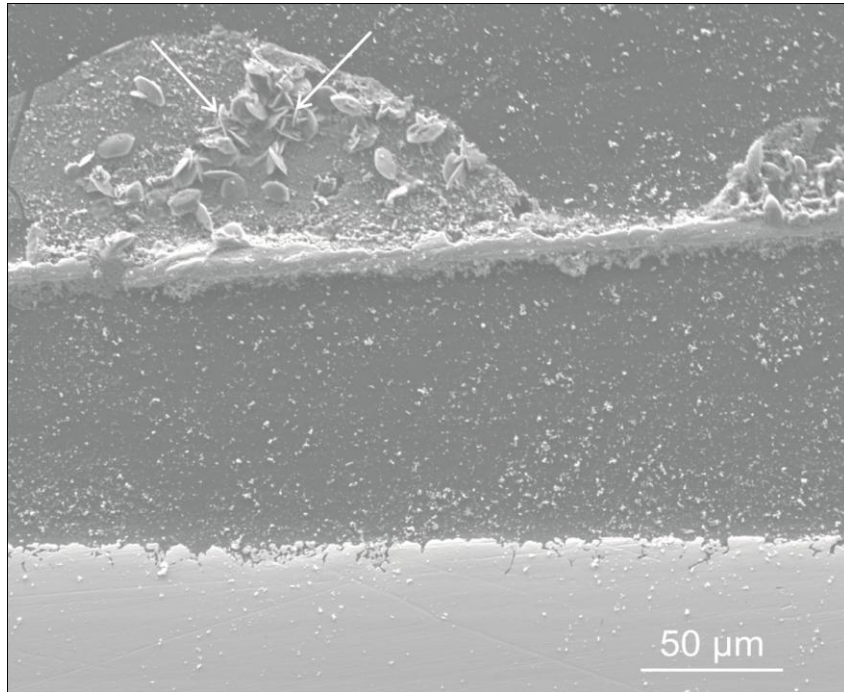
Figure 11: SEM image of cross section of Type 309 steel. Arrows point to salt crystals.
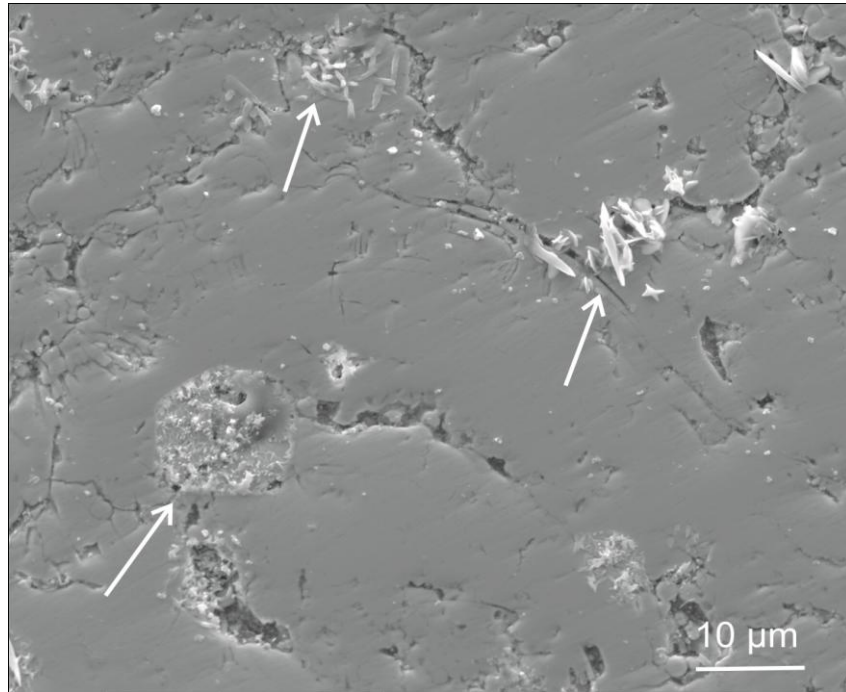
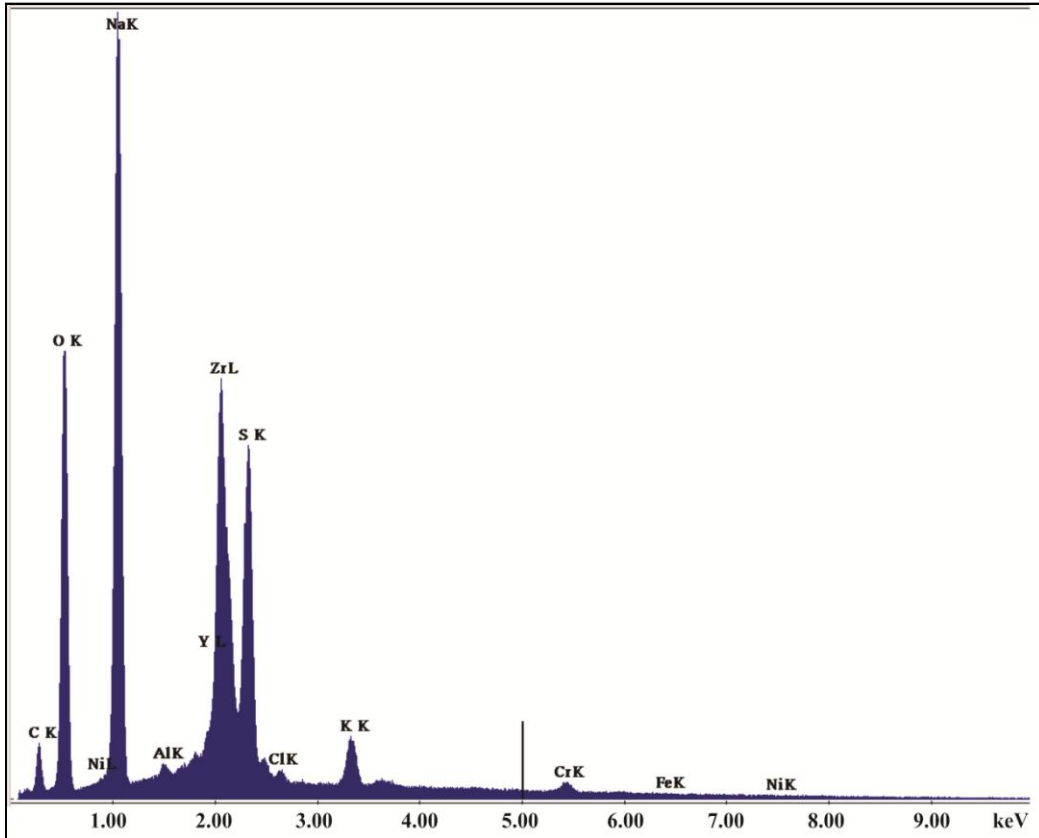**Figure 12(a):** Salt crystals oozing out of cracks of conventional YSZ coating. Arrows point to salt crystals.

Figure 12(b): EDS spectrum of salt crystals in the conventional YSZ top coat
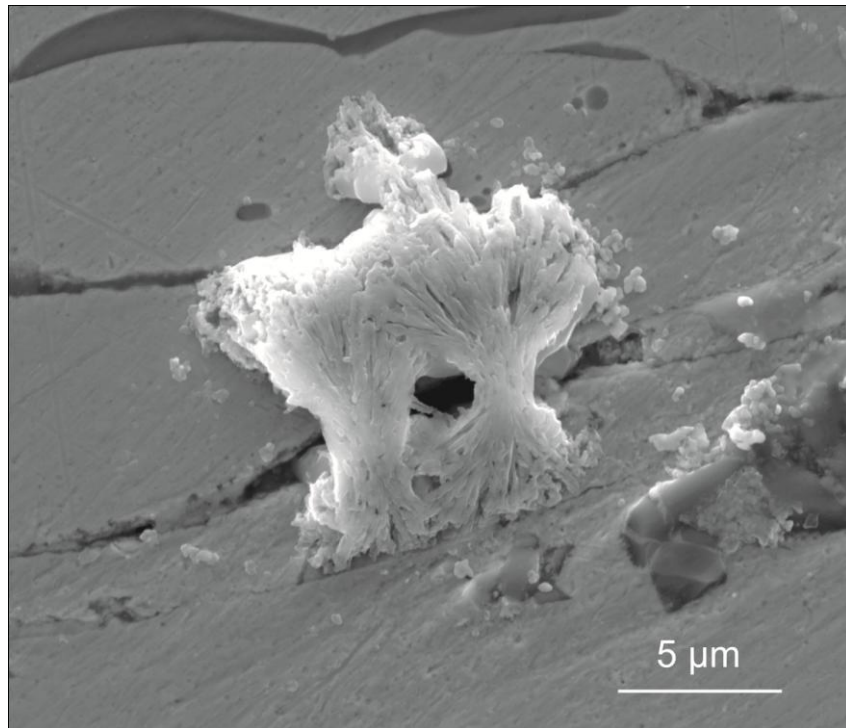
Figure 12(c): Salt crystal at the interface of bond coat and substrate of conventional YSZ coating
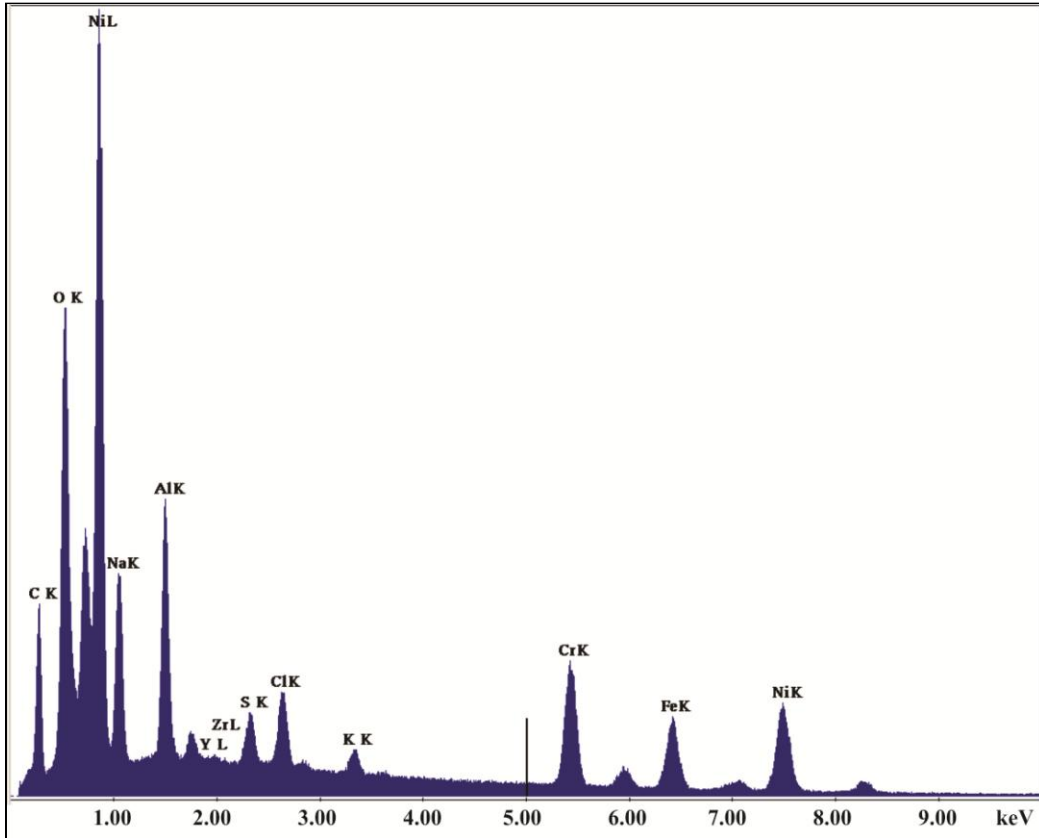
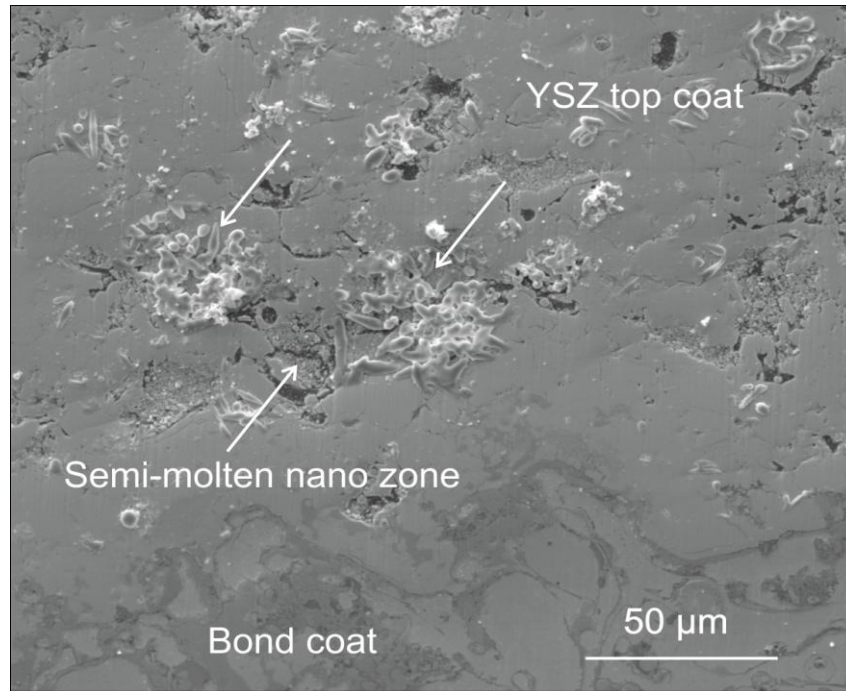**Figure 12(d):** EDS spectrum of conventional YSZ top coat SEM image shown in Fig. 12c.

Figure 13(a): SEM image of cross section of nanostructured YSZ coating. Arrows point to salt crystals.
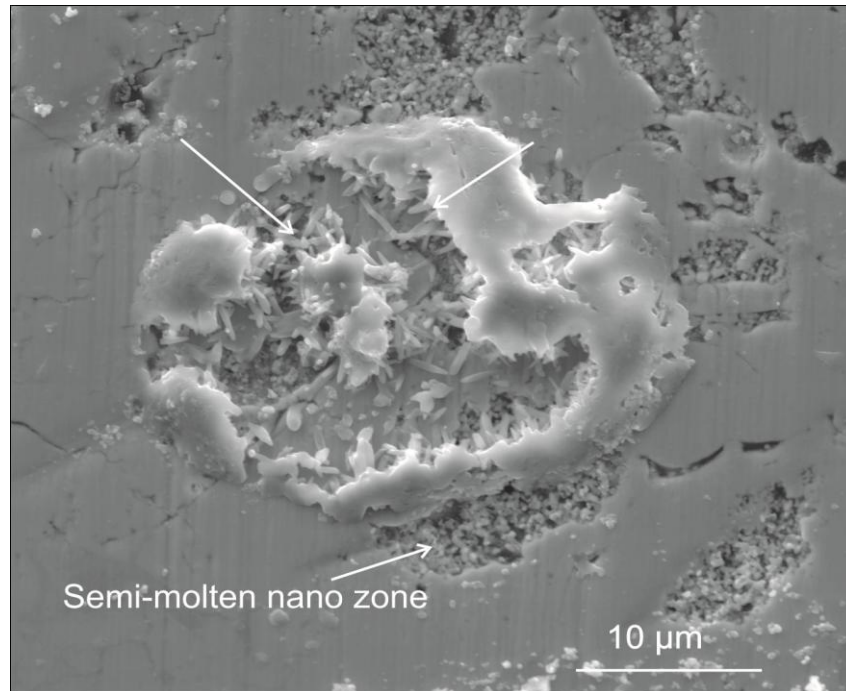
Figure 13(b): Salt crystal crystallizing in nano zones. Arrows point to salt crystals.
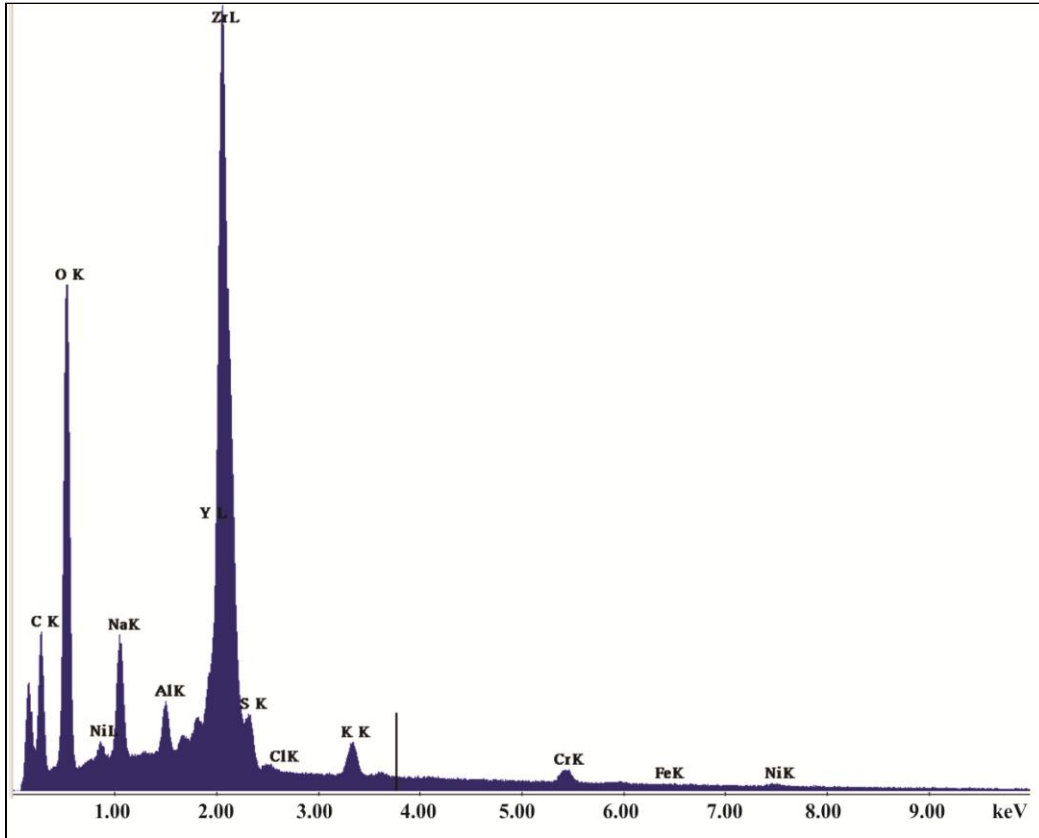
Figure 13(c): EDS spectrum of salt crystals in nano –YSZ top coat shown in Fig. 13(b)

Test C

Test C involved exposing the samples to molten salts in the presence of flue gases. Figure 14 shows the corrosion scale that has peeled from the bare steel substrate. In this case, it was found that the steel had been attacked by intergranular corrosion [6]

Similar to Test B, salt crystals were found mainly in cracks in the conventional based YSZ top coat. This can be seen from Fig. 15a where the salt crystals are shown by white arrows. These crystals were also found in the interface between the substrate and the bond coat over which the conventional YSZ was deposited. This is emphasized in Fig. 15b which shows a salt crystal at the interface of bond coat and steel substrate. A spot scan was conducted on this crystal and the resulting EDS spectrum is shown in Fig. 15c. From the spectrum, it is clear the the crystal shown is an NaCl crystal.

The cross sectional image of the nanostructured-based YSZ EBC from this test is shown in Fig. 16a. Similar to the previous test, it can be clearly seen that the crystals tend to crystallize in the nano zone areas of the EBC. The same phenomenon can also be seen in Fig. 16b which shows salt crystallizing in the semi-molten nano particle area. A spot scan was performed on the crystal in Fig. 16b and the resulting EDS spectrum is shown in Fig. 16c. The spectrum confirms that the crystal shown is a Na_2SO_4 crystal
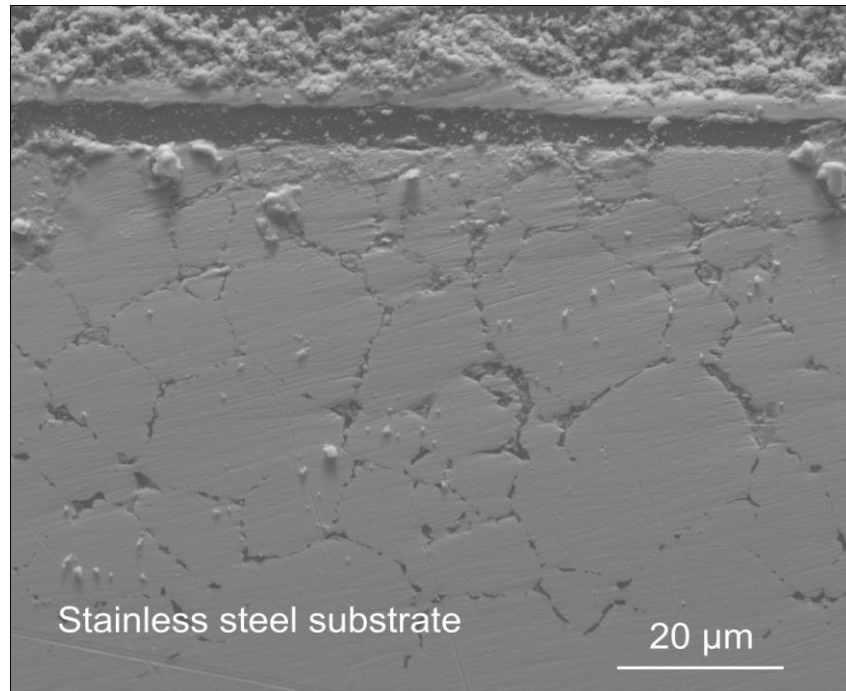
Figure 14: SEM image of cross section of Type 309 steel
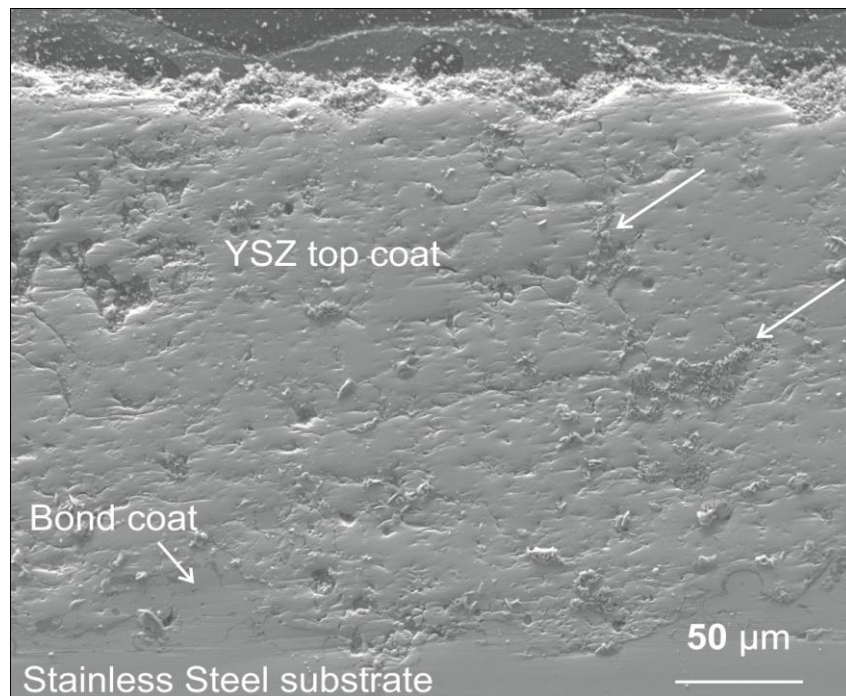
Figure 15(a): SEM image of cross section of conventional YSZ coating showing salt crystals in cracks. Arrows point to salt crystals.
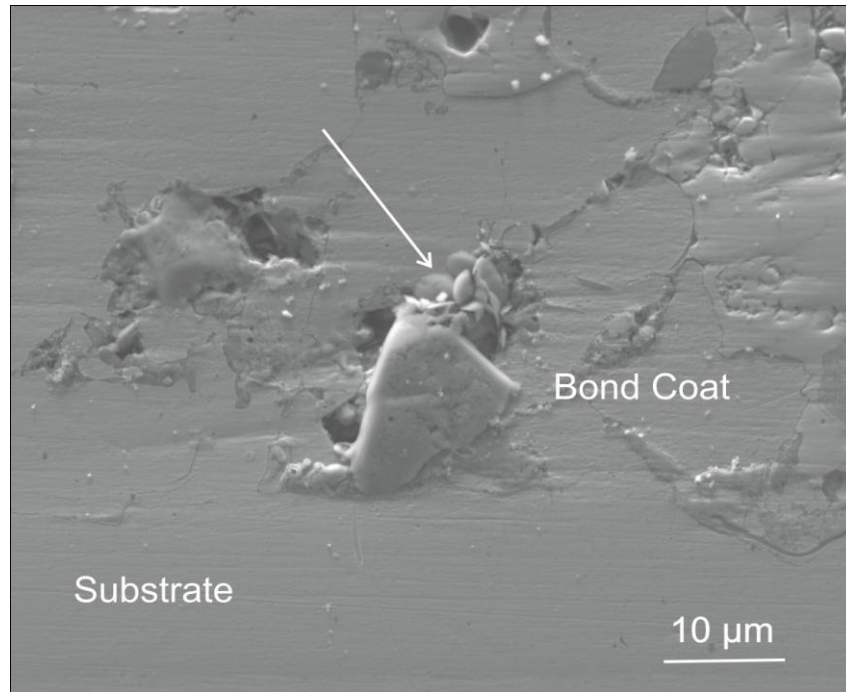
Figure 15(b): Salt crystal at the interface of bond coat and substrate of conventional YSZ coating. Arrow points to salt crystals.
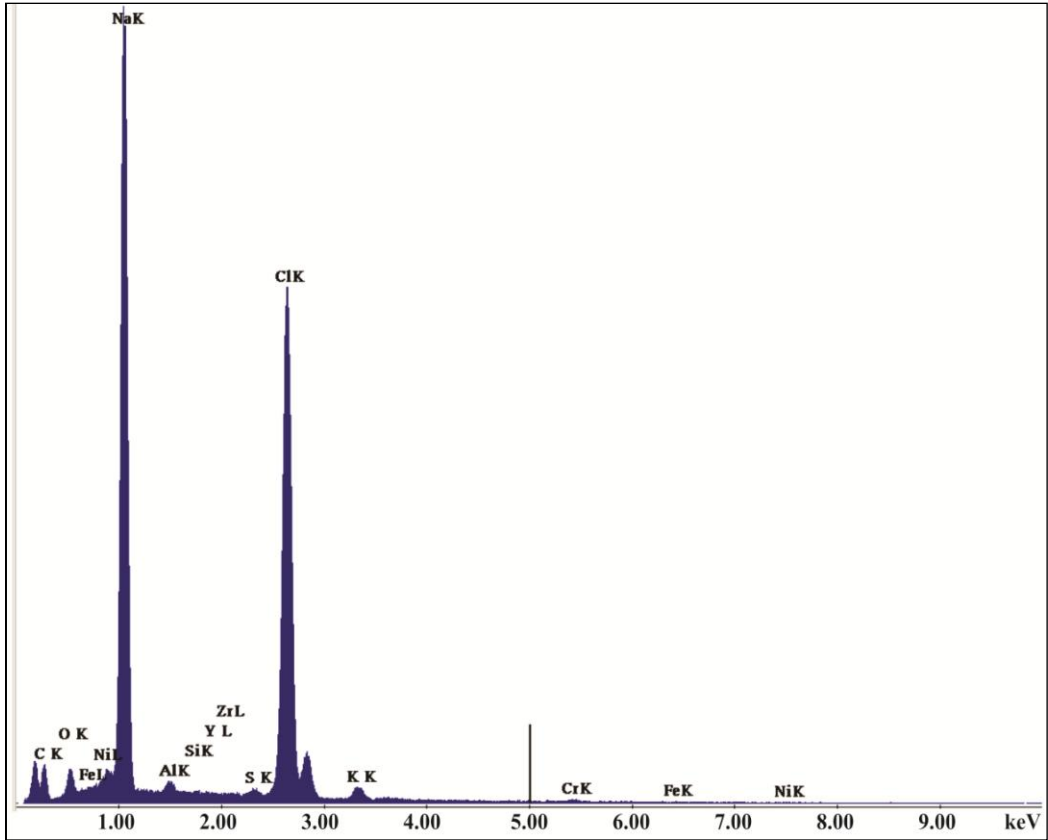
Figure 15(c): EDS spectrum of salt crystal at the interface of bond coat and substrate in conventional YSZ sample shown in Fig. 15(b).

Figure 16(a):SEM image of cross section of nanostructured YSZ coating. Arrow points to a salt crystal.

Figure 16(b): Salt crystal oozing out of nanozone of nanostructured YSZ coating.
Arrow points to a salt crystal.

Figure 16(c): EDS image of salt crystal in nano YSZ top coat shown in Fig. 16(b).

Figure 17: Nanostructured YSZ coating showing salt crystals in nano zone areas. Arrows point to salt crystals.

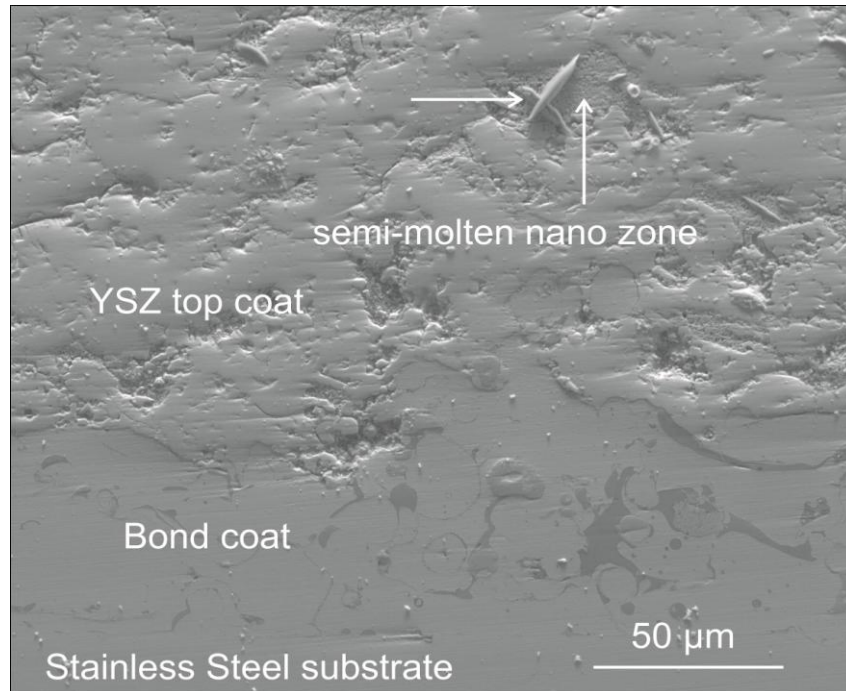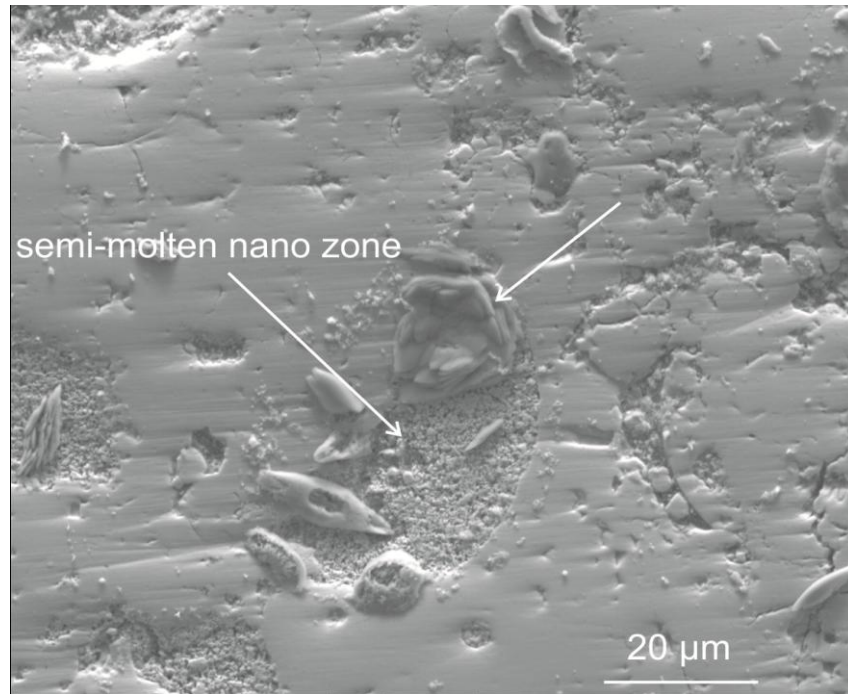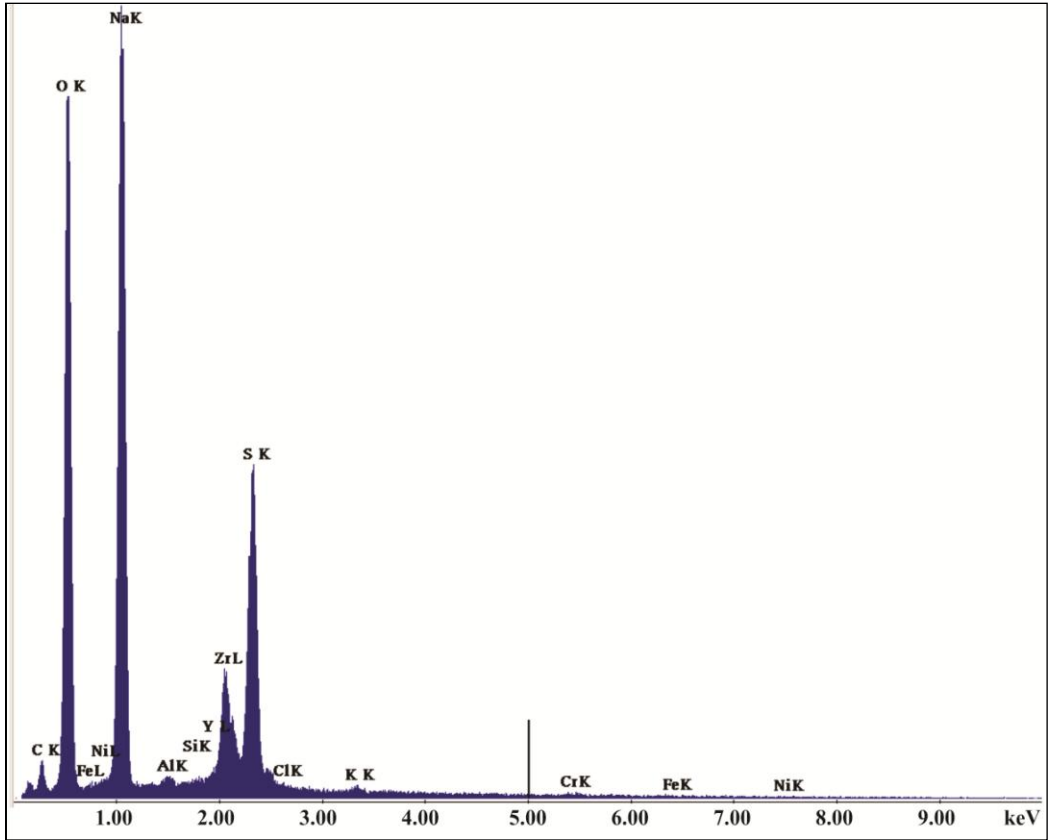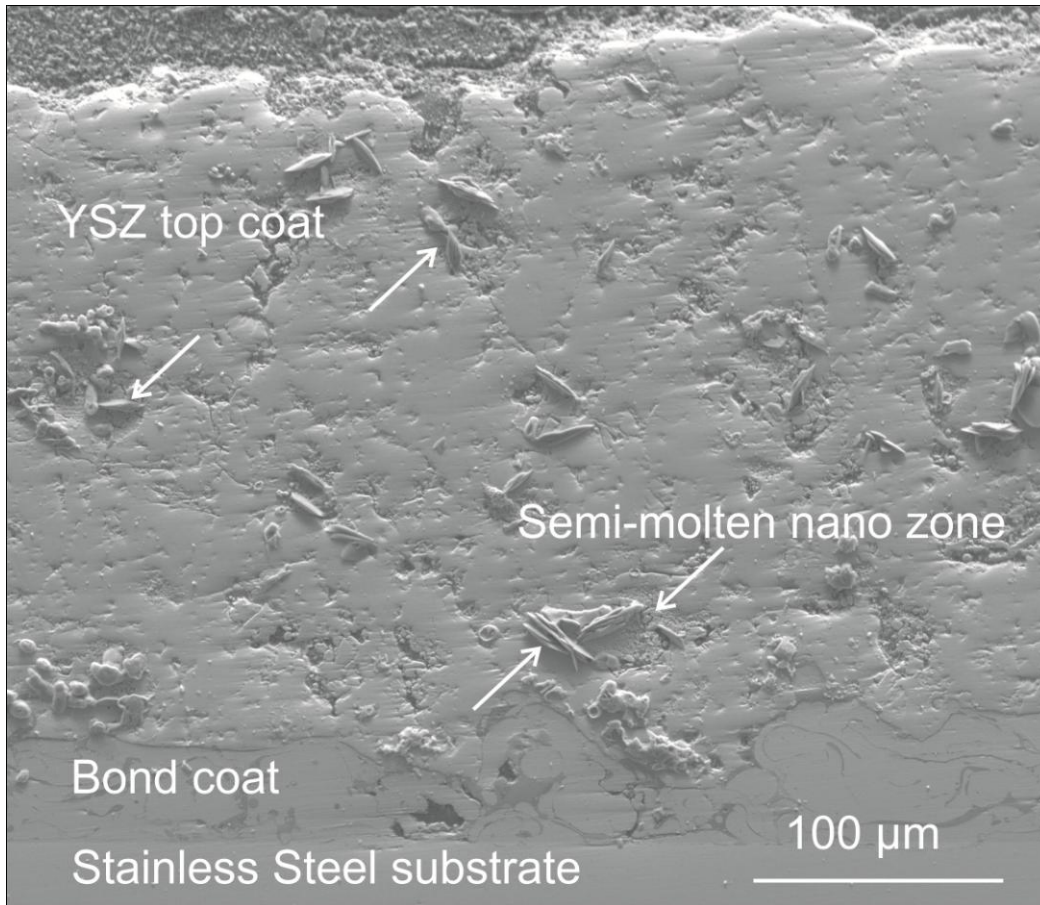## 4.4 **Discussion**

SEM/EDS

All three tests showed the presence of salt crystals in the bond coat near the steel substrate protected by the conventional YSZ coating while no salt was detected in the bond coat of either sample protected by the nanostructured YSZ coating. Semi-molten nano-particle agglomerates are embedded in the microstructure of the nanostructured YSZ coatings. It has been hypothesized that these semi-molten nano particles act as crack arresters and hence the nano-coatings are tougher than their conventional counterparts [4]. This results in fewer and smaller cracks in nanostructured YSZ coating. In this study, it was found that the salt crystals were found primarily in the area of these nanozones in the nanostructured coating while the crystals appear to have originated from the cracks in the conventional YSZ coating. Figures 13a, 13b, 16a and 16c show the presence of salt crystals in the nano-zone areas. Figures 12a and 15a show salt crystals present in cracks in the conventional YSZ top coat. A possible explanation for this phenomenon may be that these nanozones act as collection points for the molten salt penetrating through the network of cracks and pores in the coating. Once the samples cool, the salts crystallize in these nanozone areas. On the other hand, given that there are no nanoparticles present in the conventional YSZ coating, the molten salt continues to penetrate through the inter-connected cracks in the conventional coating until it reaches the denser bond coat/substrate interface. This explains the presence of salt crystals near the surface of the substrate protected by the conventional YSZ coating.

In all the cross section SEM images shown, it appears that the salt has oozed out of cracks and the semi-molten nanozone areas. This is because once the samples are exposed to the ambient air, the moisture in the atmosphere draws these crystals out. Hence, these crystals appear to have oozed out of cracks and nanozone areas.

Figure 10 in Chapter 3 shows an EDS image of a conventional YSZ coating exposed to NaCl salt at 600°C. Note the absence of salt in cracks in the coating in this figure. This contrasts with the SEM images in this Chapter where we find the presence of salt in cracks and in nanozone areas. The reason behind this phenomenon could be that NaCl salt did not melt at 600°C while some of the synthetic salt mixture did. As a result, the molten salt penetrated into the cracks of the coating while NaCl remained at the top, as indicated by the EDS image. Had polishing been a reason for redeposition of salt, then NaCl would have been inside the coating as well. Hence, polishing is not a likely reason for the redeposition of the salts inside cracks and in nanozones in the coating.

Salts crystallizing in cracks in the conventional YSZ top coat may also have detrimental effects on the mechanical strength of the coating. A possible analogy that can be made here is that of weathering of rocks due to salt crystallization. Salt crystal growth can exert tremendous pressure and is known to pry loose individual minerals in a rock. This phenomenon is particularly effective in porous, granular rocks like sandstone [7]. As these crystals grow in the cracks, they wedge the rock apart. Similarly, as these crystals grow in the cracks of the conventional YSZ top coat, they may cause more stresses in the coating. In the

case of the nanostructured YSZ-based EBC, it was found that the salt crystals are present primarily in the nano-zone areas. This can be confirmed from Fig. 17, which shows the presence of salt crystals in the nanozone areas. It can also be seen that there are hardly any salt crystals present in the cracks of the coating. This could result in lower stresses as the cracks are not being wedged apart due to the growing crystals in this case.

The bare steel samples in all tests have been attacked violently and to a greater degree in comparison to the coated samples (see Figs. 8, 11 and 14). Interestingly, the bare steel in test C (Fig. 14) has experienced intergranular corrosion. This was not observed in test B (Fig. 11) and Test A(Fig. 8). A possible explanation for this phenomenon could be the presence of chlorine in an environment containing water vapor. Austenitic stainless steels that are heated into or slowly cooled through the 500ºC to 800ºC temperature range are susceptible to intergranular corrosion under certain conditions [6]. Water vapor, which acts as an electrolyte aiding in the corrosion process was not present in Test B. Hence, the stainless steel in this case did not exhibit intergranular corrosion.

Although the stainless steel samples behaved differently to the flue gas/salt mixture test as compared to the air/salt mixture test, no such differences in behavior was observed for any of the coating samples.

**XRD**

Metastable tetragonal phase (*t'*-phase) is the most desirable phase for the integrity of YSZ plasma-sprayed coatings [8]. The metastable tetragonal phase is identified by analysing the 72° to 75° region of the 2θ co-ordinate on the XRD

profiles of YSZ. The (004) and (220) peaks in this region is associated with the metastable t' phase [8]. Figure 18 shows this region of the XRD pattern of the powders while Fig. 19 shows the same for the as sprayed coatings. The two peaks present in the XRD pattern for powders are also present in the as sprayed coating pattern. This indicates that the non transformable t'-phase has been retained in the as sprayed coating. Previous studies conducted on phase changes in YSZ coatings after annealing them to temperatures above 1000ºC have shown that the t' phase decomposes into the equilibrium t, cubic c and monoclinic m phases. In our study, the samples were heated only to 600ºC for 168 hours. Hence, it was expected that the metastable t' phase would be retained. XRD patterns of samples from Test B and Test C are shown in Figs. 20 and 21. It was found that the (004) and (220) peaks were still present in the XRD patterns of the samples, indicating that the t'-phase was retained after exposure to the corrosive environment. Longer duration tests in the same environment would be necessary to study the effect of the corrosive environment on the phase transformation of YSZ.

A slight difference in peak positions (peak shifts) is observed between the conventional YSZ coatings and nanostructures YSZ coatings. Shift in peak positions might be related to microstrains or different yttria contents [9]. The conventional YSZ feedstock powder (Metco 204NS-G, Sulzer Metco, Inc., Westbury, NY, USA) consisted of 8wt% yttria while the nanostructured YSZ feedstock powder (Nanox Powder S4007, Inframat Corporation, Farmington, CT, USA) consisted of 7wt% yttria. This could be a possible reason for the shift in peak positions.
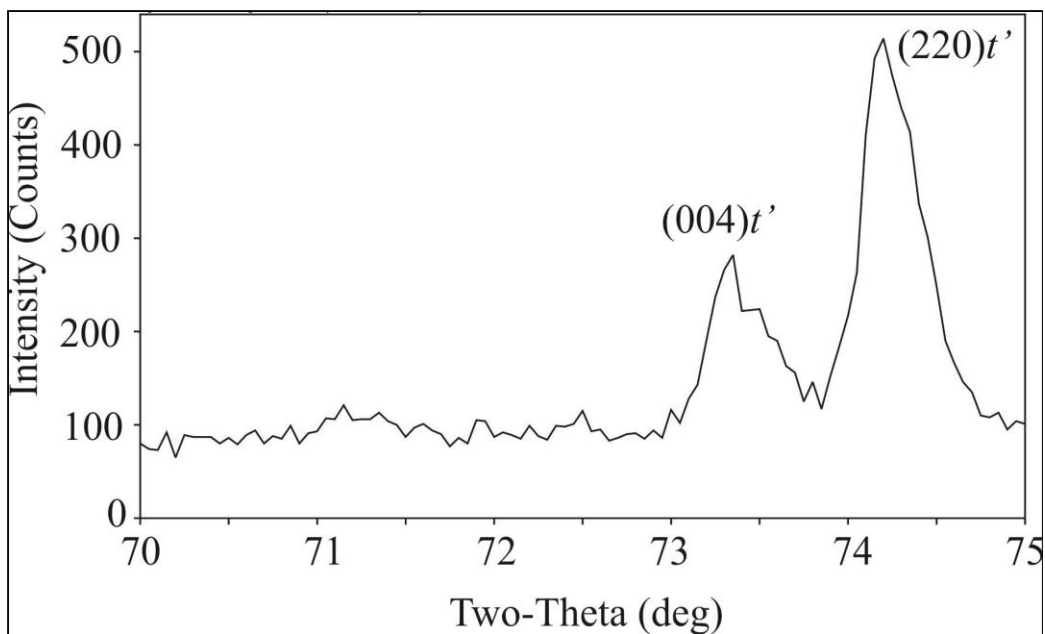
(a)
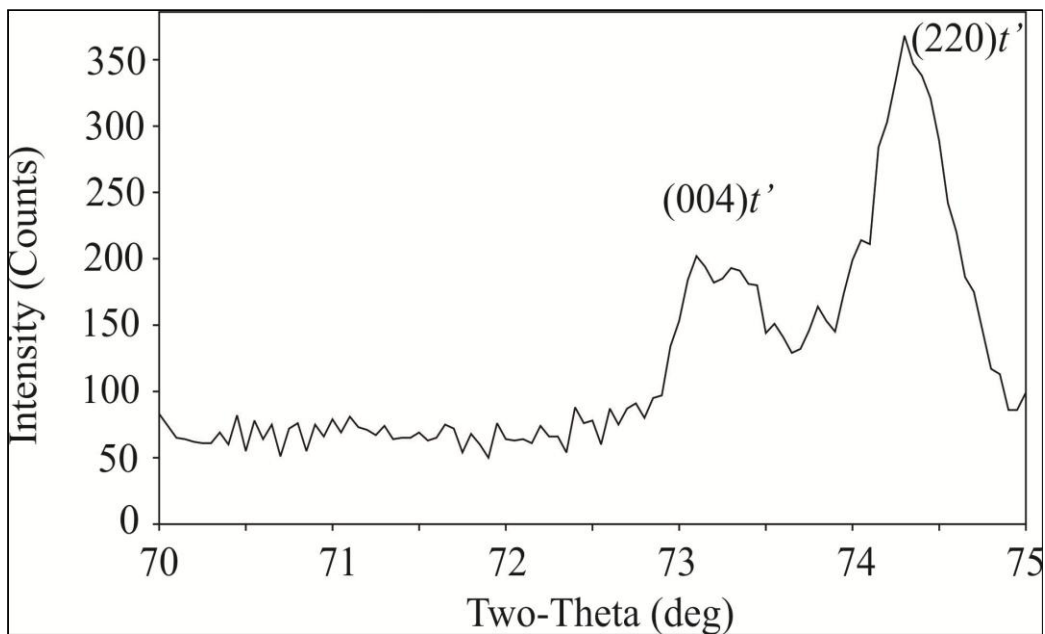
(b)

Figure 18: XRD pattern of (a) conventional (b) nano-structured YSZ powder
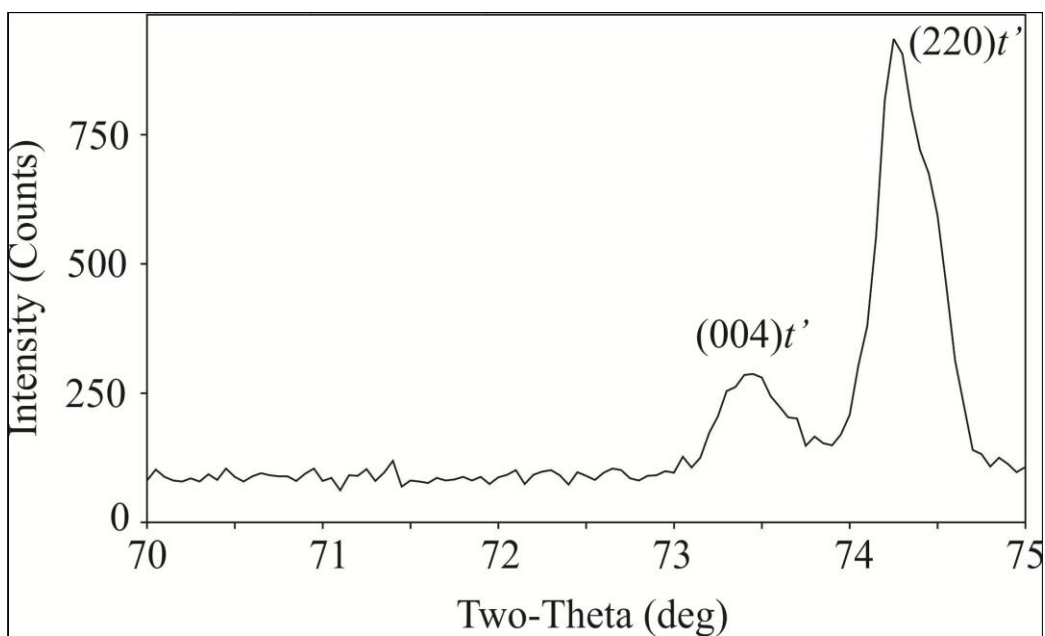
(a)
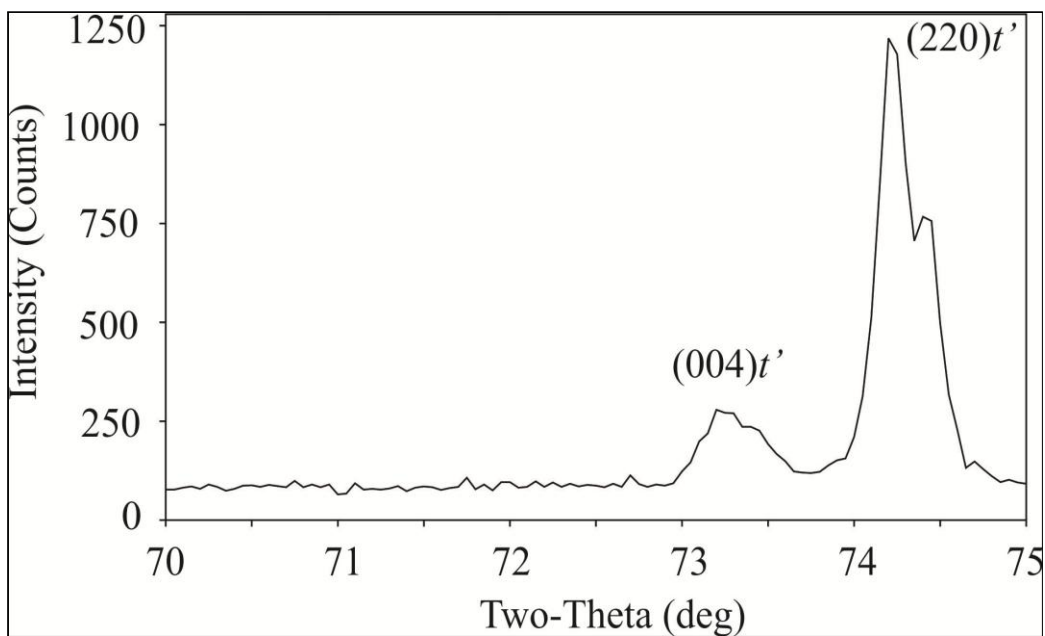
(b)

Figure 19: XRD pattern of as-sprayed (a) conventional (b) nano-structured YSZ coatings

(a)

(b)

Figure 20: XRD pattern of (a) conventional YSZ coating and (b) nanostructured YSZ coating from test B (600°C, air, synthetic salt mixture)
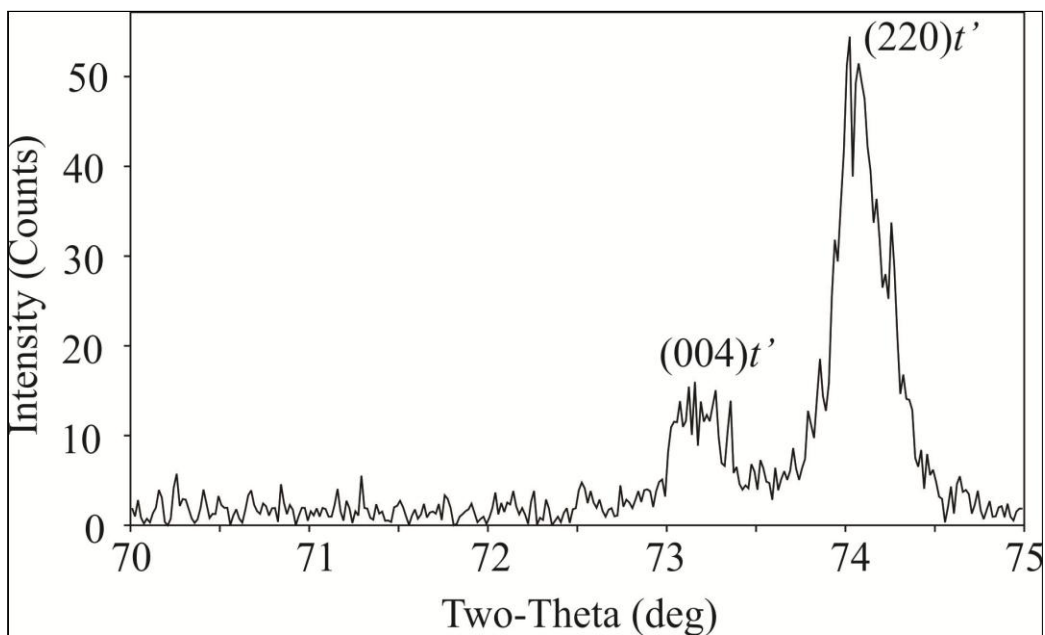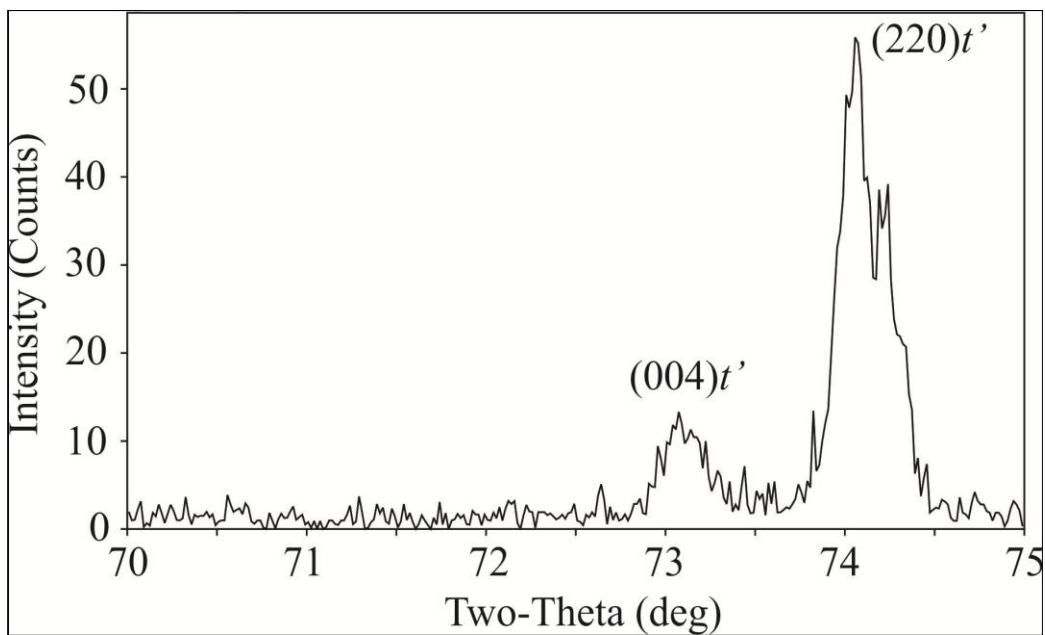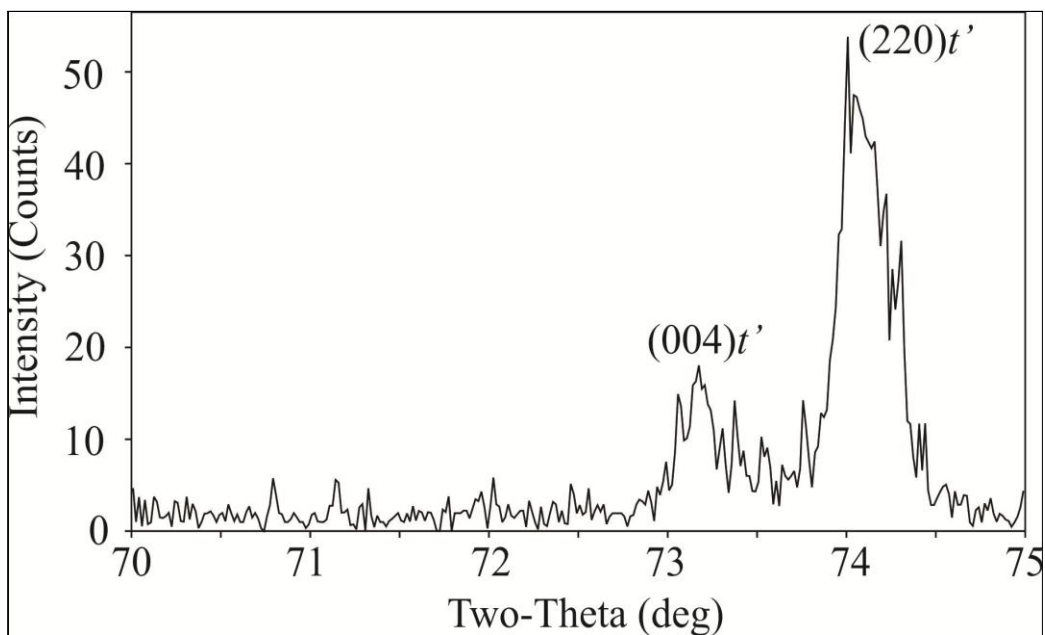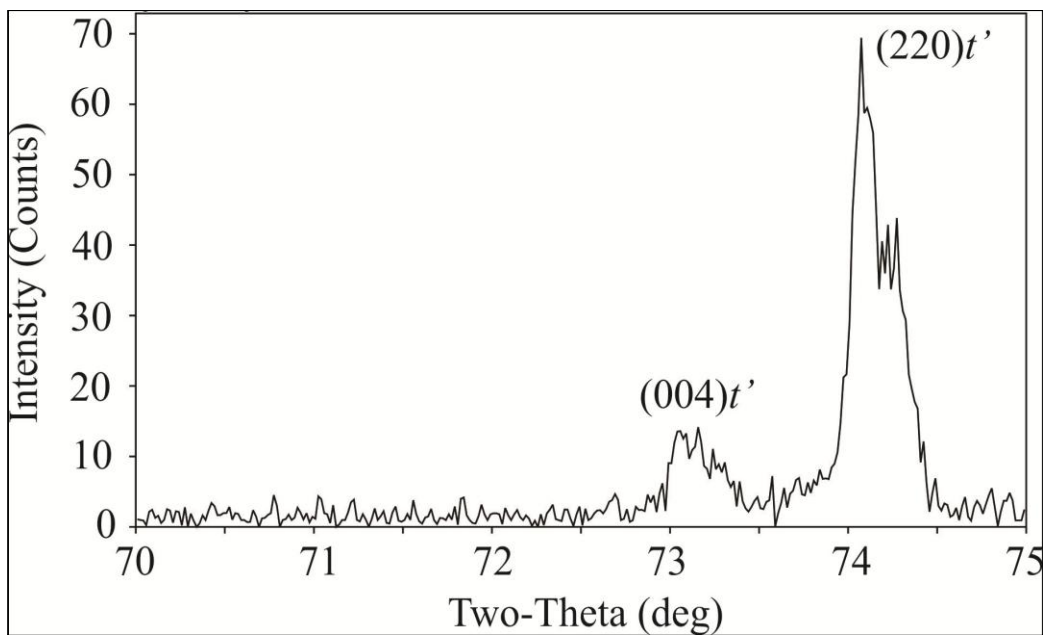
(a)

(b)

Figure 21: XRD pattern of (a) conventional YSZ coating and (b) nanostructured YSZ coating from test C (600°C, flue gas, synthetic salt mixture)

4.5 **Conclusion**

Plasma-sprayed environmental barrier coatings (EBC) based on conventional and nanostructured yttria-stabilized zirconia (YSZ) top coats were exposed to corrosive molten salts and simulated boiler flue gases. It was found that the nanostructured-based YSZ EBC provided improved protection to the underlying steel substrate in comparison to the conventional-based YSZ EBC. This was attributed to the presence of semi-molten nanoparticles in the coating and the collection of salt material in these nanozones. Conventional YSZ coatings do not have these semi-molten particles in their microstrucure and hence, salt penetrates through the cracks till they reach the denser bond coat/ substrate.

The non transformable tetragonal prime (t') phase, which is the most desirable phase for YSZ coatings, has been retained in the coatings after the corrosion tests. This behavior was expected since the temperature of exposure was not high enough for the t' phase to decompose into the cubic (c) and equilibrium tetragonal (t) phases.

Additional analysis will be required to explain the impact of the aggressive molten salt/flue gas mixture on the EBC and transport through the coating/substrate system. Longer duration tests would be required to check whether the nanostructured YSZ coating continues to be impenetrable by the salts at the bond coat level.

4.6 **References**

[1]   H. Fujikawa and H. Makiura, "Corrosion behavior of various steels in black liquor recovery boiler environment," *Materials and Corrosion*, vol. 50, Mar. 1999, pp. 154-161.

[2]   A.S. Osyka, A.I. Rybnikov, S.A. Leontiev, N.V. Nikitin, and I.S. Malashenko, "Experience with metal/ceramic coating in stationary gas turbines," *Surface and Coatings Technology*, vol. 76-77, Nov. 1995, pp. 86-94.

[3]   R.S. Lima and B.R. Marple, "Nanostructured YSZ thermal barrier coatings engineered to counteract sintering effects," *Materials Science and Engineering: A*, vol. 485, Jun. 2008, pp. 182-193.

[4]   R.S. Lima and B.R. Marple, "Thermal Spray Coatings Engineered from Nanostructured Ceramic Agglomerated Powders for Structural, Thermal Barrier and Biomedical Applications: A Review," *Journal of Thermal Spray Technology*, vol. 16, Mar. 2007, pp. 40-63.

[5]   T.N. Adams, W.J. Frederick, T.M. Grace, M. Hupa, K. Lisa, A.K. Jones, and H. Tran, "Upper Furnace Deposition and Plugging," *Kraft Recovery Boilers*, 1997, pp. 247-282.

[6]   W.F. Smith and J. Hashemi, "Intergranular Corrosion," *Foundations of Materials Science and Engineering*, New York: McGraw-Hill, 2006, pp. 751-753.

[7]   B. Pipkin, D.D. Trent, R. Hazlett, and P. Bierman, "Physical Weathering," *Geology and the Environment*, Belmont: Thomson Learning, 2008, pp. 150-151.

[8]   K. Muraleedharan, J. Subrahmanyam, and S.B. Bhaduri, "Identification of t' Phase in ZrO_2-7.5 wt% Y_2O_3 Thermal-Barrier Coatings," *Journal of the American Ceramic Society*, vol. 71, 1988, pp. 226-227.

[9]   G. Di Girolamo, C. Blasi, L. Pagnotta, and M. Schioppa, "Phase evolution and thermophysical properties of plasma sprayed thick zirconia coatings after annealing," *Ceramics International*, vol. 36, Dec. 2010, pp. 2273-2280.

5 Conclusion

Atmospheric plasma sprayed yttria-stabilized zirconia (YSZ) samples were tested for their corrosion resistance for use in the superheater section of a recovery boiler. The performance of conventional YSZ environmental barrier coating (EBC) and nanostructured YSZ EBC was compared. The samples were exposed to different environments at 600°C in a furnace.

In the preliminary test described in Chapter 3, the samples were exposed to NaCl salt at 600°C in the presence of medical grade air. They were kept in the furnace for a total period of 76 hrs. The Scanning Electron Microscope (SEM) images of the cross section of the coatings were reported. No penetration of NaCl salt into the YSZ ceramic was found. The cross section of the nanostructured YSZ ceramic clearly showed fewer cracks as compared to the conventional based YSZ top coat. A possible reason for this phenomenon could be that the semi-molten nano particles present in the microstructure of the nano coating acted as crack arresters [1]. This has been previously reported in literature. This means that the nanostructured YSZ coating offers better mechanical strength and crack resistance as compared to the conventional YSZ coating. Although spallation of the coatings were not observed after exposure for 76 hrs, wider and larger number of cracks in the conventional YSZ coating suggests that the chances of failure are much higher in the conventional based EBC than the nanostructured EBC. It was also observed that the coating with a thicker ceramic layer had more cracks than a coating with a

thinner one. A possible explanation for this phenomenon could be that more stresses are induced in a thicker ceramic coating as compared to a thinner one. The large thermal expansion mismatch between the steel substrate and the thicker ceramic top coat might be a possible explanation for higher stresses in a thicker EBC.

In the molten salt corrosion test described in Chapter 4, the samples were exposed to three different environments – salt vapor and flue gases, molten salt and air, molten salt and flue gases. The samples were kept in a furnace maintained at 600°C for a period of 168 hrs. A synthetic salt mixture with a first melting point of around 520°C was used. This ensured that some amount of salt was in molten state and this allowed it to penetrate into the porous ceramic top coat. The resistance of the conventional YSZ top coat and nanostructured YSZ top coat to the movement of molten salt was examined. In all three different environment tests conducted, salt crystals could be seen in the SEM images of the cross section of both the conventional and nano YSZ coatings. The crystals appeared to have penetrated to the interface between the substrate and boat coat over which conventional YSZ top coat was deposited. This was not observed in the nano-YSZ coating. This means that the nano YSZ protected the steel substrate better than its conventional counterpart under the specified environment conditions. The salt crystals were also observed in cracks in the conventional YSZ top coat while they tended to crystallize in nano zone areas in the nanostructured coating. The crystallization of salt in cracks may tend to wedge the cracks apart and this is detrimental to the mechanical strength of the coating. The absence of these

crystals in the cracks present in the nano coating indicates that this coating can offer better mechanical strength due to the absence of stresses induced in the coating by crystallization of salts in cracks.

X ray diffraction analysis was performed on all samples in the preliminary test as well as the molten salt tests. The presence of metastable tetragonal phase (t' − phase) was found in all the samples after exposure. The t' − phase is the most desirable phase for the integrity of these plasma sprayed coatings. The presence of this phase after the tests indicated that the ceramic did not undergo transformation to the equilibrium tetragonal and cubic phase.

A heat transfer model was prepared to check the impact of the ceramic YSZ coating on the heat transfer in the super heater section of a recovery boiler. The model described in Chapter 2 shows that there is negligible impact of the YSZ ceramic on the heat transfer process. Hence, the application of YSZ coating to mitigate corrosion of superheater tubes might be a good solution to the problem of tube failures.

5.1　Future Work

1. Field research

Although laboratory tests and results provide a good indication about the performance of these coatings, testing these samples in an actual recovery boiler would give us a better insight into their behavior. In an actual boiler, the coatings would be exposed to the hot sulphidic gases and also to the hot molten inorganic salts. These conditions would subject the coatings to an extremely corrosive

environment and their performance here would be a true indication of their ability to resist corrosion.

2. Longer duration tests

In the current study, the samples were exposed to the corrosive environment for a maximum period of 168 hrs. Recovery boilers run continuously for 4 to 6 months before they are shut down for maintanence purposes. Hence, although the nanostructured YSZ coating did exhibit better resistance to the movement of salt and protected the substrate better than its conventional counterpart, longer duration tests of at least 4 months would be required to check whether the nano coating continues to be impenetrable to the salts at the bond coat level.

5.2   References

[1]   R.S. Lima and B.R. Marple, "Nanostructured YSZ thermal barrier coatings engineered to counteract sintering effects," *Materials Science and Engineering: A*, vol. 485, Jun. 2008, pp. 182-193.